Cell Reports

Report

mTOR Signaling and SREBP Activity Increase FADS2 Expression and Can Activate Sapienate Biosynthesis

Graphical Abstract

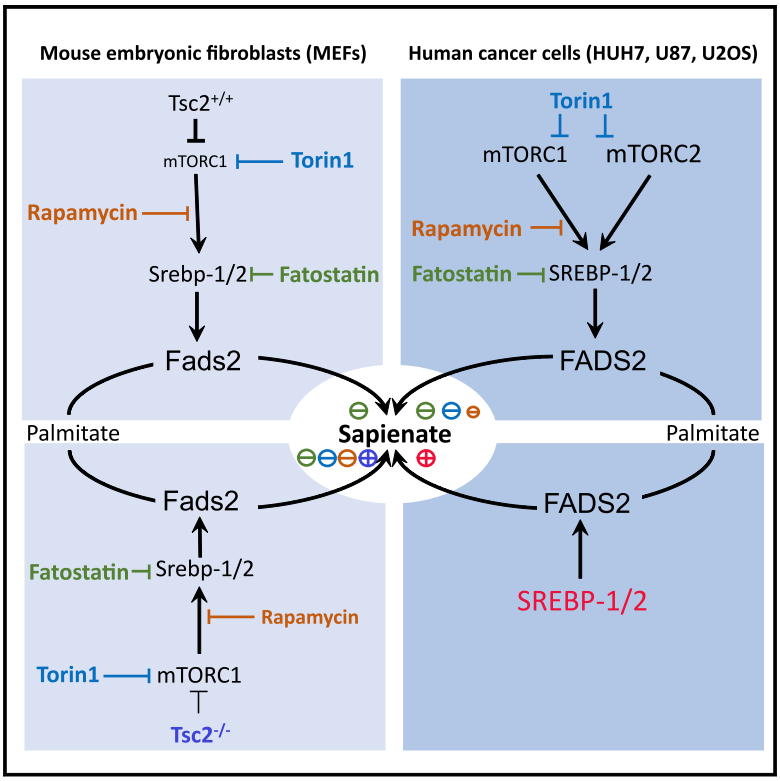

Highlights

- *FADS2* expression is prognostic in some cancers
- *FADS2* is a target of SREBP-1 and SREBP-2
- SREBP activity and mTOR signaling regulate FADS2-mediated sapienate metabolism
- Torin1 treatment reduces *FADS2* expression and sapienate metabolism in xenografts

Authors

Mouna Triki, Gianmarco Rinaldi, Melanie Planque, ..., Thomas G.P. Grünewald, Almut Schulze, Sarah-Maria Fendt

Correspondence

sarah-maria.fendt@kuleuven.vib.be

In Brief

Triki et al. report that *FADS2* expression is prognostic in some cancers and that FADS2-mediated sapienate metabolism is regulated by mTOR signaling. Mechanistically, *FADS2* is a target of SREBP-1/2. Inhibition of mTOR or SREBP reduces *FADS2* expression and sapienate metabolism in cancer cells and liver xenografts.

Triki et al., 2020, Cell Reports *31*, 107806
June 23, 2020
https://doi.org/10.1016/j.celrep.2020.107806

CellPress

Cell Reports

CellPress
OPEN ACCESS

Report

mTOR Signaling and SREBP Activity Increase FADS2 Expression and Can Activate Sapienate Biosynthesis

Mouna Triki,[1,2] Gianmarco Rinaldi,[1,2] Melanie Planque,[1,2] Dorien Broekaert,[1,2] Alina M. Winkelkotte,[3,4] Carina R. Maier,[5] Sudha Janaki Raman,[5] Anke Vandekeere,[1,2] Joke Van Elsen,[1,2] Martin F. Orth,[6] Thomas G.P. Grünewald,[6,7,8,9] Almut Schulze,[3,5] and Sarah-Maria Fendt[1,2,10,*]

[1]Laboratory of Cellular Metabolism and Metabolic Regulation, VIB-KU Leuven Center for Cancer Biology, VIB, Herestraat 49, 3000 Leuven, Belgium
[2]Laboratory of Cellular Metabolism and Metabolic Regulation, Department of Oncology, KU Leuven and Leuven Cancer Institute (LKI), Herestraat 49, 3000 Leuven, Belgium
[3]Division of Tumor Metabolism and Microenvironment, German Cancer Research Center, Im Neuenheimer Feld 581, 69120 Heidelberg, Germany
[4]Faculty of Biosciences, University of Heidelberg, 69120 Heidelberg, Germany
[5]Biochemistry and Molecular Biology, Theodor-Boveri-Institute, Biocenter, Am Hubland, 97074 Würzburg, Germany
[6]Max-Eder Research Group for Pediatric Sarcoma Biology, Institute of Pathology, Faculty of Medicine, LMU Munich, Thalkirchner Strasse 36, 80337 Munich, Germany
[7]German Cancer Consortium (DKTK), partner site Munich, 80337 Munich, Germany
[8]Division of Translational Pediatric Sarcoma Research, German Cancer Research Center (DKFZ), Im Neuenheimer Feld 280, 69120 Heidelberg, Germany
[9]Institute of Pathology, Heidelberg University Hospital, Im Neuenheimer Feld 224, 69120 Heidelberg, Germany
[10]Lead Contact
*Correspondence: sarah-maria.fendt@kuleuven.vib.be
https://doi.org/10.1016/j.celrep.2020.107806

SUMMARY

Cancer cells display an increased plasticity in their lipid metabolism, which includes the conversion of palmitate to sapienate via the enzyme fatty acid desaturase 2 (FADS2). We find that FADS2 expression correlates with mammalian target of rapamycin (mTOR) signaling and sterol regulatory element-binding protein 1 (SREBP-1) activity across multiple cancer types and is prognostic in some cancer types. Accordingly, activating mTOR signaling by deleting tuberous sclerosis complex 2 (*Tsc2*) or overexpression of *SREBP-1/2* is sufficient to increase *FADS2* mRNA expression and sapienate metabolism in mouse embryonic fibroblasts (MEFs) and U87 glioblastoma cells, respectively. Conversely, inhibiting mTOR signaling decreases FADS2 expression and sapienate biosynthesis in MEFs with Tsc2 deletion, HUH7 hepatocellular carcinoma cells, and orthotopic HUH7 liver xenografts. In conclusion, we show that mTOR signaling and SREBP activity are sufficient to activate sapienate metabolism by increasing *FADS2* expression. Consequently, targeting mTOR signaling can reduce sapienate metabolism *in vivo*.

INTRODUCTION

Metabolic changes are a hallmark of cancer cells (Hanahan and Weinberg, 2011). One such change is a deregulated lipid metabolism, which is frequently found in many cancers (Currie et al., 2013). Alterations in lipid metabolism can serve the increased proliferation needs of cancer cells, because they are important building blocks of cell membranes (Röhrig and Schulze, 2016). Lipid metabolism alterations observed in cancer cells include elevated *de novo* synthesis of fatty acids, increased fatty acid uptake, and activated processing of fatty acids, including desaturation (Peck and Schulze, 2016). Recently, we discovered that some cancers, such as liver and lung carcinomas, have an increased plasticity in their lipid metabolism (Vriens et al., 2019). These cancers not only rely on the well-described stearoyl-coenzyme A (stearoyl-CoA) desaturase (SCD)-dependent pathway that generates the monounsaturated fatty acids palmitoleate and oleate (Peck et al., 2016) but also repurpose the enzyme fatty acid desaturase 2 (FADS2) to generate the unusual fatty acid sapienate (Vriens et al., 2019). Accordingly, sapienate can replace palmitoleate in cell membranes. While sapienate metabolism can sustain proliferation in cancers upon SCD inhibition, most cancer cells competent in using sapienate metabolism, already activate this pathway in parallel with the well-described SCD pathway (Vriens et al., 2019). Thus, this raises the question how sapienate metabolism is regulated in cancer cells.

An important regulator of fatty acid metabolism is sterol regulatory element-binding protein 1/2 (SREBP-1/2), which has been

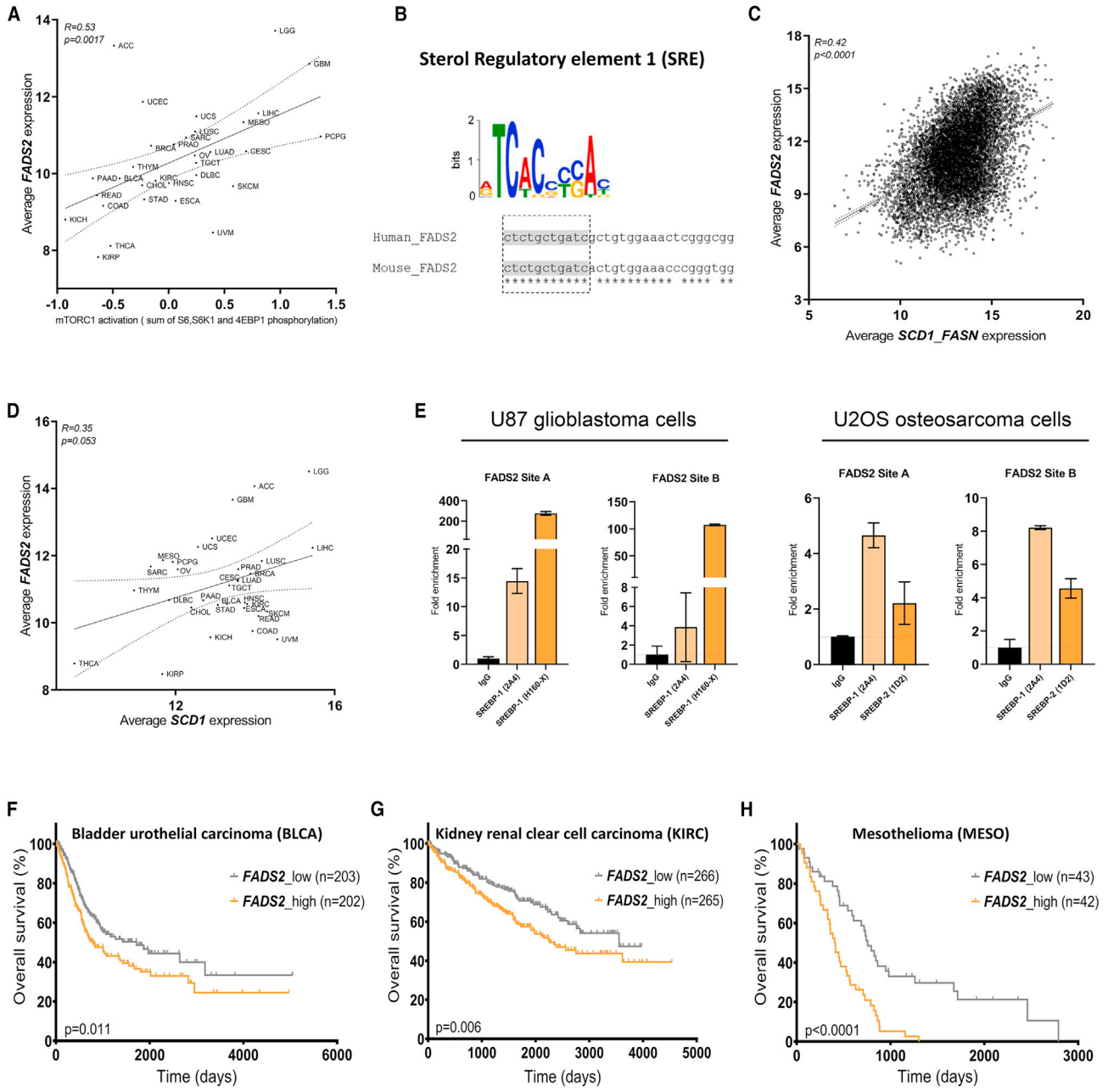

Figure 1. *FADS2* mRNA Expression Correlates with mTORC1 Signaling and SREBP-1 Activity and Has Prognostic Value

(A) Correlation between *FADS2* mRNA expression and mTOR activity in 7,407 human cancers representing 32 different cancer type. Reverse-phase protein array (RPPA) profiles were scored for an mTOR pathway signature, defined as the sum of phosphoprotein levels of mTOR, 4E-BP1 (S65, T37/T46, and T70 RPPA features), P70S6K, and S6 (S235/S236 and S240/S244 features). Trend line (dashed line) and 95% confidence intervals (dotted lines) are depicted.

(B) Conserved regions for the sterol regulatory element 1 (SRE) consensus sequence in human and mouse *FADS2* promoter region are highlighted in gray, while identical nucleotides are indicated with asterisks.

(C) Correlation between *FADS2* mRNA expression and SREBP-1 targets (*SCD1* and *FASN*) across 9,185 human cancers representing 32 major tumor types. Trend line (dashed line) and 95% confidence intervals (dotted lines) are depicted.

(D) Correlation between *FADS2* and *SCD1* mRNA expression in 9,185 human cancers representing 32 major tumor types. Trend line (dashed line) and 95% confidence intervals (dotted lines) are depicted.

(E) ChIP-qPCR assay using anti-SREBP-1 and anti-SREBP-2 antibodies to detect enriched gene-promoter fragments of *FADS2* in U87 (left panel) and U2OS (right panel) cancer cells. IgG was used as ChIP control. Values represent relative increase of real-time PCR signals compared with the signal of IgG ChIP. Three technical triplicates are presented as mean ± SD.

(legend continued on next page)

shown to activate transcription of enzymes, including ATP citrate lyase (ACLY), acetyl-CoA carboxylase 1 (ACC1), fatty acid synthase (FASN), elongation of very-long-chain fatty acids (ELOVL), SCD1, and the fatty acid transporter CD36 (Madison, 2016; Mossmann et al., 2018). Interestingly, in fish and mouse, SREBP-1 has also been shown to regulate Fads2 mRNA expression in conjunction with biosynthesis of long-chain polyunsaturated fatty acids (Dong et al., 2017; Matsuzaka et al., 2002). Yet, whether SREBPs plays an important role in FADS2-mediated sapienate metabolism in cancer remains unknown.

A relevant signaling protein upstream of SREBPs is mammalian target of rapamycin (mTOR), which has also been shown to be important for cancer cell proliferation (Ben-Sahra and Manning, 2017; Eid et al., 2017; Lorendeau et al., 2015; Porstmann et al., 2008). mTOR is a serine/threonine-specific protein kinase that exists in two complexes named mTORC1 and mTORC2 (Laplante and Sabatini, 2012). One upstream negative regulator of mTORC1 is tuberous sclerosis complex 1/2 (TSC1/2) (Manning and Cantley, 2003; Wong, 2010). While mTORC1 and C2 can have individual downstream substrates, they both can activate SREBP-1. On the one hand, mTORC1 can exert regulation on SREBP-1 activity via activation of S6 kinase 1 (S6K1) or inhibition of phosphatidate phosphatase LPIN1 (LIPIN 1) (Mossmann et al., 2018). On the other hand, mTORC2 can control SREBP-1 activity via AKT signaling (Mossmann et al., 2018). Moreover, mTOR signaling can modulate COPII-dependent SREBP-1 processing via CREB regulated transcription coactivator 2 (CRTC2) (Han et al., 2015). While the close interconnection between SREBP-1 and mTOR signaling is established, it remains elusive whether modulation of mTOR signaling can alter *FADS2* expression and sapienate metabolism in transformed cells.

Here, we addressed the question whether mTOR signaling and SREBP-1/2 activity can alter sapienate metabolism by modulating *FADS2* mRNA expression in (cancer) cells. We find that both mTOR and SREBP inhibition can decrease *FADS2* mRNA expression and sapienate metabolism in transformed cells and tumors with activated mTOR growth signaling.

RESULTS

FADS2 mRNA Expression Correlates with mTORC1 Signaling and SREBP-1 Activity

mTORC1 is an important regulator of lipid metabolism (Lorendeau et al., 2015). Therefore, we asked whether there is evidence that mTORC1 signaling is also involved in the regulation of FADS2-mediated sapienate metabolism. To address this question, we correlated mTORC1 activity, defined by S6, S6K1, and eukaryotic translation initiation factor 4E-binding protein 1 (4E-BP1) phosphorylation (Saxton and Sabatini, 2017), with *FADS2* mRNA expression based on The Cancer Genome Atlas (TCGA) data from 7,407 human cancers representing 32 major tumor types. Interestingly, we found a significant positive correlation between mTORC1 activity and *FADS2* mRNA expression (Figure 1A; Table S1).

Next, we asked which component of the mTORC1 signaling cascade could potentially regulate *FADS2* mRNA expression. To identify such components, we performed an *in silico* binding motif analysis and identified the SREBP-1 consensus sequence in the *FADS2* promotor of humans and mice (Figure 1B). Accordingly, SREBP-1 activity, defined by *SCD1* and fatty acid synthase (*FASN*) expression (Mossmann et al., 2018), was significantly correlated with *FADS2* expression based on TCGA data across 9,185 human cancers representing 32 major tumor types (Figure 1C; Table S2). Moreover, *FADS2* expression was found to be correlated with *SCD1* expression based on TCGA data from 9,185 human cancers representing 32 major tumor types (Figure 1D; Table S3). These results suggest *FADS2* being a SREBP-1 target, which is supported by previous research (Lewis et al., 2015). To confirm this hypothesis, we performed chromatin immunoprecipitation (ChIP) qPCR of *FADS2* with SREBP-1 or SREBP-2 in glioblastoma (U87) and osteosarcoma (U2OS) cells and found that indeed SREBP-1 and SREBP-2 bind the FADS2 promotor in these human cancer cells (Figure 1E). Thus, this identifies *FADS2* as an SREBP-1 and SREBP-2 target.

In addition, we correlated *FADS2* expression with copy-number alterations, somatic mutations, and deletions of major oncogenes or tumor suppressors (*MYC*, *PTEN*, *TP53*, and *PIK3CA*) based on TCGA data from human cancers representing 33 major tumor types (Figures S1A and S1B; Table S4) and found significant correlations depending on the tumor type. Moreover, *FADS2* transcription was prognostic for bladder urothelial carcinoma, kidney renal clear cell carcinoma, and mesothelioma (Figures 1F–1H).

Based on these data, we concluded that *FADS2* expression can correlate with driver events of an oncogenic transformation, mTOR signaling and SREBP activity. In line, we confirmed *FADS2* as a target of SREBP-1 and SREBP-2 and found that *FADS2* expression is prognostic in some cancers.

mTORC1 Signaling Can Increase Fads2 Expression and Sapienate Metabolism

Next, we hypothesized that mTORC1 signaling can increase *FADS2* transcription and consequently sapienate metabolism in cells. To address this hypothesis, we used immortalized mouse embryonic fibroblasts (MEFs) and the corresponding

(F) Kaplan-Meier survival curves based on low (gray curve) or high (orange curve) mRNA expression of *FADS2* in bladder urothelial carcinoma (BLCA), kidney renal cell carcinoma (KIRC) and mesothelioma (MESO). Significance for differential overall survival of the two groups was assessed with the Mantel-Haenszel test. ACC, adrenocortical carcinoma; BLCA, bladder urothelial carcinoma; BRCA, breast invasive carcinoma; CESC, cervical squamous cell carcinoma and endocervical adenocarcinoma; CHOL, cholangiocarcinoma; COAD, colon adenocarcinoma; DLBC, lymphoid neoplasm diffuse large B cell lymphoma; ESCA, esophageal carcinoma; GBM, glioblastoma multiforme; HNSC, head and neck squamous cell carcinoma; KICH, kidney chromophobe; KIRC, kidney renal clear cell carcinoma; KIRP, kidney renal papillary cell carcinoma; LAML, acute myeloid leukemia; LGG, brain lower-grade glioma; LIHC, liver hepatocellular carcinoma; LUAD, lung adenocarcinoma; LUSC, lung squamous cell carcinoma; MESO, mesothelioma; OV, ovarian serous cystadenocarcinoma; PAAD, pancreatic adenocarcinoma; PCPG, pheochromocytoma and paraganglioma; PRAD, prostate adenocarcinoma; READ, rectum adenocarcinoma; SARC, sarcoma; SKCM, skin cutaneous melanoma; STAD, stomach adenocarcinoma; TGCT, testicular germ cell tumors; THCA, thyroid carcinoma; THYM, thymoma; UCEC, uterine corpus endometrial carcinoma; UCS, uterine carcinosarcoma; UVM, uveal melanoma.

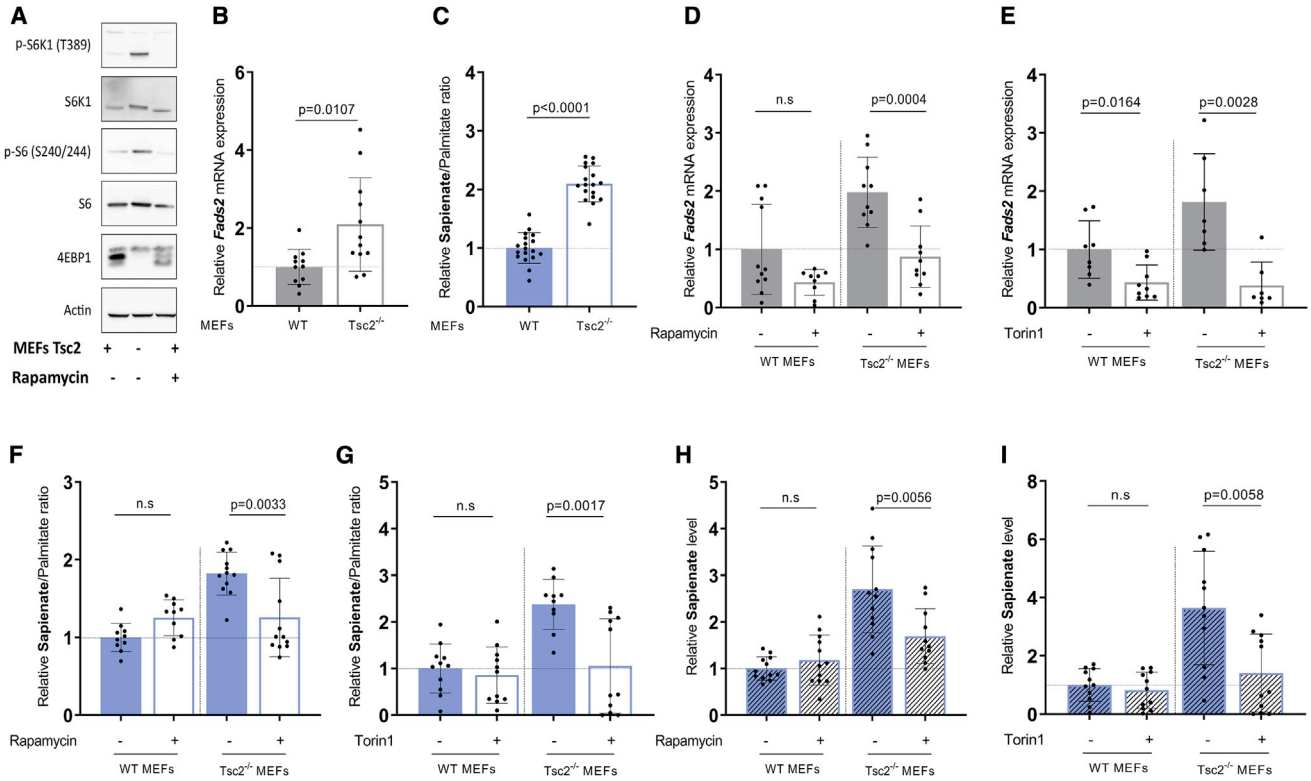

Figure 2. mTOR Can Regulate *Fads2* Expression and Sapienate Metabolism

(A) Representative western blot of mTORC1 activity in wild-type (WT) and Tsc2$^{-/-}$ MEFs. mTORC1 activity was analyzed by immunoblotting with the indicated antibodies.

(B) Relative *Fads2* mRNA expression in WT (n = 11) and Tsc2$^{-/-}$ (n = 12) MEFs based on qRT-PCR. Bar graphs are presented as mean ± SD from biological independent samples. Statistical testing was performed by a two-sided unpaired Student's t test.

(C) Relative sapienate to palmitate ratio in WT and Tsc2$^{-/-}$ MEFs based on mass spectrometry analysis. n = 18. Bar graphs are presented as mean ± SD from biological independent samples. Statistical testing was performed by a two-sided unpaired Student's t test.

(D and E) Relative *Fads2* mRNA expression in WT and Tsc2$^{-/-}$ MEFs upon treatment with DMSO (D: WT n = 11, Tsc2$^{-/-}$ n = 10; E: WT n = 8, Tsc2$^{-/-}$ n = 7), rapamycin (D) (20 nM, 72 h, WT n = 9, Tsc2$^{-/-}$ n = 10), or Torin1 (E) (40 nM, 72 h, WT n = 9, Tsc2$^{-/-}$ n = 7). Bar graphs are presented as mean ± SD from biological independent samples. Statistical testing was performed by a two-sided unpaired Student's t test.

(F and G) Sapienate to palmitate ratio in WT and Tsc2$^{-/-}$ MEFs upon treatment with DMSO (F: WT N = 11, Tsc2$^{-/-}$ n = 12; G: WT n = 11, Tsc2$^{-/-}$ n = 10), rapamycin (F) (20 nM, 72 h, WT n = 10, Tsc2$^{-/-}$ n = 12), or Torin1 (G) (40 nM, 72 h, WT n = 11, Tsc2$^{-/-}$ n = 11). Bar graphs are presented as mean ± SD from biological independent samples. Statistical testing was performed by a two-sided unpaired Student's t test.

(H and I) Relative sapienate level in WT and Tsc2$^{-/-}$ MEFs upon treatment with DMSO (H: n = 12; I: n = 11), rapamycin (H) (20 nM, 72 h, n = 12), or Torin1 (I) (40 nM, 72 h, n = 11). Bar graphs are presented as mean ± SD from biological independent samples. Statistical testing was performed by a two-sided unpaired Student's t test.

MEFs with deletion of Tsc2 (Tsc2$^{-/-}$), which results in the hyperactivation of mTORC1 signaling (Figure 2A). Subsequently, we measured *Fads2* mRNA expression and sapienate biosynthesis based on the sapienate to palmitate ratio (Vriens et al., 2019) with qPCR and mass spectrometry, respectively. We observed a significant increase in *Fads2* expression and an elevation of the sapienate to palmitate ratio in Tsc2$^{-/-}$ compared to control MEFs (Figures 2B and 2C). Based on these data, we concluded that activation of mTORC1 signaling increases *Fads2* expression and sapienate metabolism.

Inhibiting mTOR Signaling Reduces FADS2 Expression and Sapienate Biosynthesis

Next, we asked whether inhibition of mTOR signaling reduces sapienate metabolism. To address this question, we treated immortalized MEFs and the corresponding Tsc2$^{-/-}$ MEFs with rapamycin or Torin1 and assessed *Fads2* transcription and sapienate biosynthesis. Notably, rapamycin inhibits part of the canonical mTORC1 signaling, while Torin1 inhibits both mTORC1 and mTORC2 (Zheng and Jiang, 2015). We found that rapamycin and more pronounced Torin1 decreased *Fads2* mRNA expression in Tsc2$^{-/-}$ MEFs, while Torin1 also significantly decreased *Fads2* expression in Tsc2 wild-type MEFs (Figures 2D and 2E). However, only in Tsc2$^{-/-}$ MEFs was the downregulation of *Fads2* expression sufficient to decrease the sapienate to palmitate ratio and sapienate levels (but not palmitate levels) (Figures 2F–2I, S2A, and S2B). Next, we assessed sapienate metabolism in HUH7 hepatocellular carcinoma cells upon rapamycin and Torin1 treatment. In line with the data from Tsc2$^{-/-}$ MEFs, we found that rapamycin

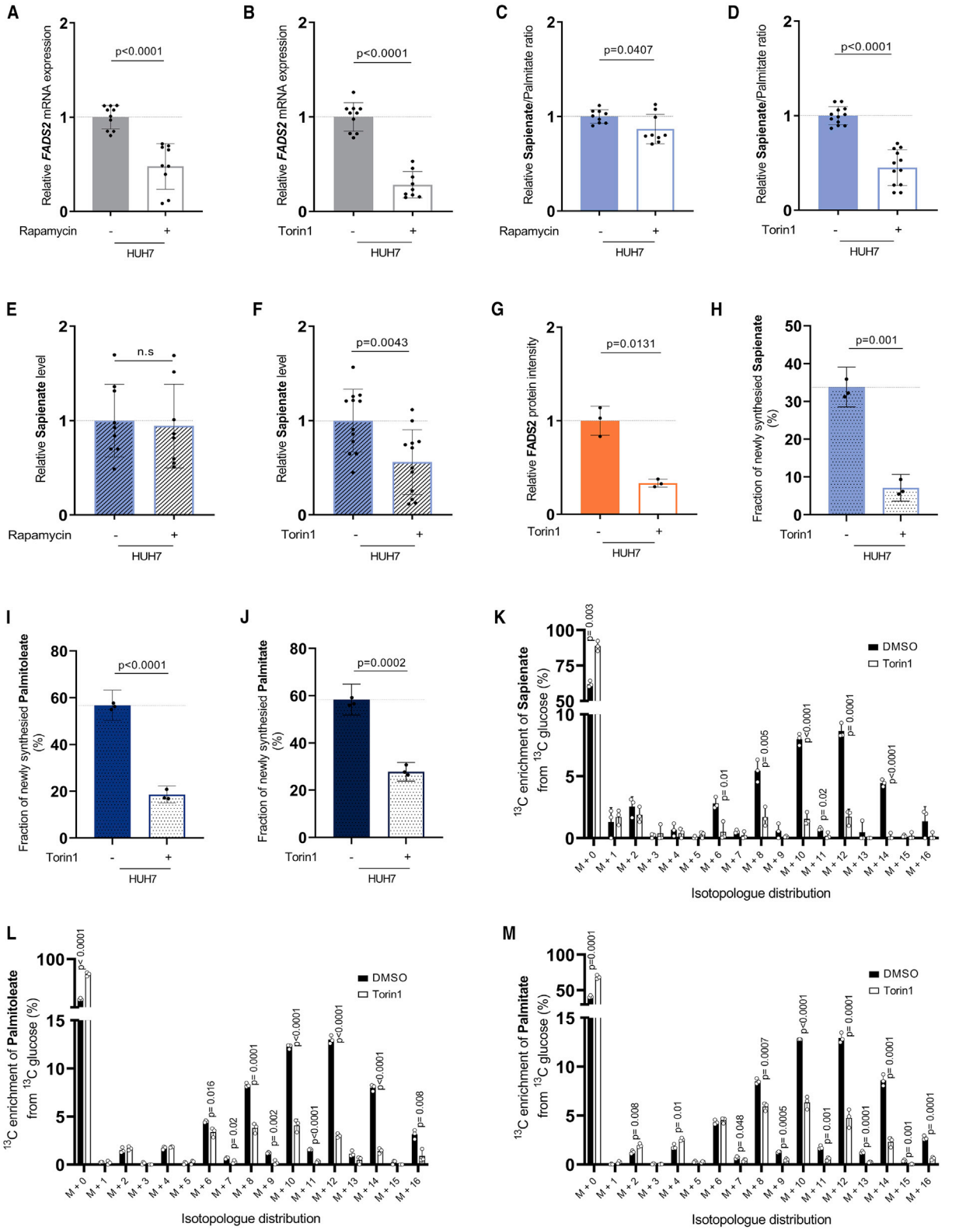

(legend on next page)

and again much more pronounced Torin1 reduced *FADS2* expression and the sapienate to palmitate ratio (Figures 3A–3D). Sapienate levels (but not palmitate levels) were only reduced upon Torin1 treatment in HUH7 cells (Figures 3E, 3F, S2C, and S2D). Additionally, we confirmed that also FADS2 protein levels were significantly reduced upon treatment with Torin1 in HUH7 cells (Figure 3G). This shows that blocking mTOR signaling decreases sapienate metabolism in transformed cells. Overall, it is important to note that Torin1 treatment (which inhibits mTORC1 and C2) had a more pronounced effect on sapienate metabolism than rapamycin.

Next, we performed ^{13}C tracer analysis using ^{13}C glucose (Buescher et al., 2015) and calculated the fraction of newly synthesized sapienate, palmitoleate, and palmitate with isotopomer spectral analysis (Yoo et al., 2004). In line with the other results, we observed that Torin1 treatment decreased the fraction of newly synthesized sapienate, palmitoleate, and palmitate (Figures 3H–3J) and reduced the incorporation of ^{13}C glucose into sapienate, palmitoleate, and palmitate in HUH7 cells (Figures 3K–3M). Importantly, the fraction of newly synthesized sapienate decreased by 4.7-fold, while the fraction of newly synthesized palmitoleate and palmitate decreased by only 3.0- and 2.1-fold, respectively (Figures 3H–3J). This shows that sapienate biosynthesis is more reduced by Torin1 treatment than explained through the reduction of palmitate synthesis.

FADS2 is involved not only in sapienate production (Vriens et al., 2019) but also in the polyunsaturation of essential fatty acids (Cho et al., 1999). Therefore, we also analyzed the levels of the polyunsaturated fatty acids linoleic acid (LA), docosahexaenoic acid (DHA), and arachidonic acid (AA) in MEFs and HUH7 cells upon Torin1 treatment. In line with the idea that mTOR signaling stimulates *de novo* fatty acid synthesis (Laplante and Sabatini, 2009), we found that the levels of polyunsaturated fatty acids (AA and DHA in MEFs and HUH7, LA in HUH7) originating from the uptake or processing of essential fatty acids (LA:AA; α-linolenic acid:DHA), were increased upon mTOR inhibition (Figures S3A–S3I). In accordance with our previous results (Vriens et al., 2019), we thus concluded that modulation of *FADS2* expression does not decrease the abundance of polyunsaturated fatty acids, likely through compensation via fatty acid uptake.

Taken together, our data are consistent with the notion that mTOR signaling can alter sapienate biosynthesis through modulation of *FADS2* expression.

Modulation of SREBPs Alters FADS2 Transcription and Sapienate Metabolism

Next, we asked whether modulating SREBP activity, which can be regulated by mTOR, alters *FADS2* mRNA expression and sapienate metabolism. To address this question, we overexpressed SREBP-1 or SREBP-2 and measured *FADS2* mRNA expression and sapienate metabolism in U87 cancer cells. In line with the ChIP-qPCR data (Figure 1E), we observed that both SREBP-1 and SREBP-2 overexpression were sufficient to increase *FADS2* expression, the sapienate to palmitate ratio, and sapienate (but not palmitate) levels (Figures 4A–4C and S4A). Consistent with our *in silico* analysis, we further found that activation of sapienate metabolism correlated with an increase in *SCD1* expression and SCD1-mediated palmitoleate metabolism in U87 glioblastoma cells overexpressing SREBP-1 or SREBP-2 (Figures 4D–4F). Based on these data, we concluded that SREBP-1 and SREBP-2 overexpression can elevate *FADS2* transcription and sapienate metabolism.

To further dissect the role of SREBPs in *FADS2* regulation, we treated immortalized MEFs and the corresponding Tsc2$^{-/-}$ MEFs as well as HUH7 hepatocellular carcinoma cells with the SREBP inhibitor fatostatin (Cheng et al., 2018). Treatment with fatostatin decreased *FADS2* expression, the sapienate to palmitate ratio, and sapienate levels (but not palmitate levels) in all tested cell lines (Figures 4G–4I, S4B, and S4C). Moreover, we confirmed that fatostatin treatment decreased FADS2 protein expression in HUH7 cells (Figure 4J). Accordingly, we found that the downregulation of sapienate metabolism correlated with a decrease in SCD1-mediated palmitoleate metabolism in immortalized MEFs and the corresponding Tsc2$^{-/-}$ MEFs as well as HUH7 cells treated with fatostatin (Figures 4K–4M). Moreover, fatostatin treatment was also effective in decreasing *Fads2* and *Scd1* expression in hypoxia (1% oxygen) (Figures S4D and S4E).

Taken together, our data show that SREBP coordinates lipid metabolism, including *FADS2* expression and sapienate metabolism, in cells.

Figure 3. Inhibition of mTOR Reduces FADS2 Transcription, Protein Expression, and Sapienate Metabolism

(A and B) Relative *FADS2* mRNA expression upon treatment with DMSO (n = 10), rapamycin (A) (20 nM, 72 h, n = 9), or Torin1 (B) (40 nM, 72 h, n = 9) in HUH7 cells. Bar graphs are presented as mean ± SD from biological independent samples. Statistical testing was performed by a two-sided unpaired Student's t test.

(C and D) Sapienate to palmitate ratio upon treatment with DMSO (C: n = 9; D: n = 12), rapamycin (C) (20 nM, 72 h, n = 9), or Torin1 (D) (40 nM, 72 h, n = 12) in HUH7 cells. Bar graphs are presented as mean ± SD from biological independent samples. Statistical testing was performed by a two-sided unpaired Student's t test.

(E and F) Relative sapienate level upon treatment with DMSO (E: n = 9; F: n = 12), rapamycin (E) (20 nM, 72 h, n = 9), or Torin1 (F) (40 nM, 72 h, n = 12) in HUH7 cells. Bar graphs are presented as mean ± SD from biological independent samples. Statistical testing was performed by a two-sided unpaired Student's t test.

(G) Relative FADS2 protein expression upon treatment with DMSO or Torin1 (40 nM, 72 h, n = 3) in HUH7 cells. Bar graphs are presented as mean ± SD from biological independent samples. Statistical testing was performed by a two-sided unpaired Student's t test.

(H–J) Fraction of newly synthesized sapienate (H), palmitoleate (I), and palmitate (J) based on isotopomer spectral analysis in the HUH7 cultured in the presence of DMSO or Torin1 with $^{13}C_6$ glucose. Cells were grown in DMEM (4.5 g/L glucose, 10% FBS), after which cells were grown for 72 h in 10% dialyzed FBS DMEM containing 4.5 g/L $^{13}C_6$ glucose supplemented with DMSO or 40 nM Torin1 (n = 3). Bar graphs are presented as lower and upper 95% confidence intervals. Statistical testing was performed by a two-sided unpaired Student's t test.

(K–M) $^{13}C_6$ glucose incorporation into sapienate (K), palmitoleate (L), and palmitate (M) in HUH7 in control condition (DMSO, black) or upon Torin1 treatment (white). Cells were grown in DMEM (4.5 g/L glucose, 10% FBS) after which cells were grown for 72 h in 10% dialyzed FBS DMEM containing 4.5 g/ L $^{13}C_6$ glucose supplemented with DMSO or 40 nM Torin1 (n = 3). Bar graphs are presented as mean ± SD from biological independent samples. Statistical testing was performed by a two-sided unpaired Student's t test.

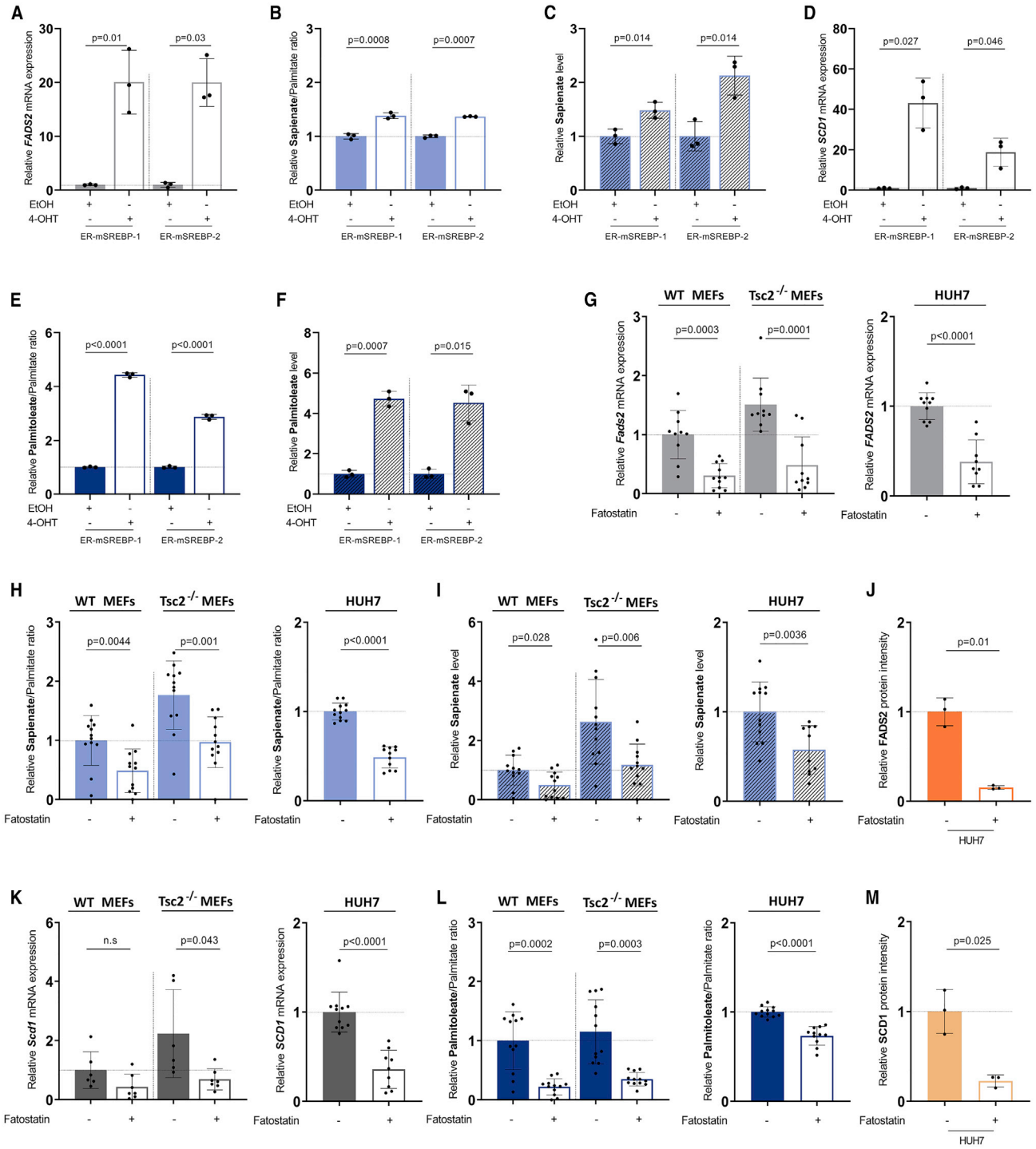

Figure 4. Modulation of SREBP Alters *FADS2* Transcription and Sapienate Metabolism

(A and D) Relative *FADS2* (A) and *SCD1* (D) mRNA expression relative to actin beta (ACTB) was determined in U87 cells stably expressing ER-mSREBP-1 or ER-mSREBP-2. Cells were treated with 100 nM 4-OHT or solvent for 24 h in medium containing 10% FBS (n = 3). Bar graphs are presented as mean ± SD from biological independent samples. Statistical testing was performed by a two-sided unpaired Student's t test.

(B and E) Sapienate to palmitate ratio (B) and palmitoleate to palmitate ratio (E) were determined in U87 cells stably expressing ER-mSREBP-1 or ER-mSREBP-2. Cells were treated with 100 nM 4-OHT or solvent for 24 h in medium containing 10% FBS (n = 3). Bar graphs are presented as mean ± SD from biological independent samples. Statistical testing was performed by a two-sided unpaired Student's t test.

(legend continued on next page)

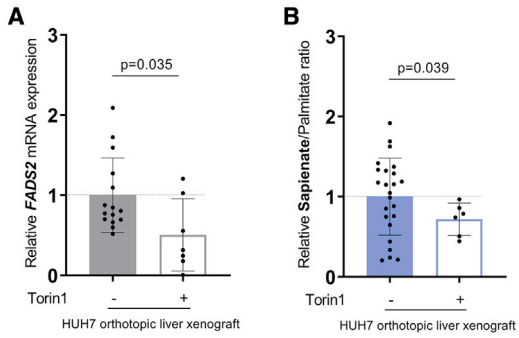

Figure 5. mTOR Inhibition Decreases Sapienate Metabolism *In Vivo*

(A) Relative *FADS2* mRNA expression in HUH7 orthotopic liver xenografts treated with vehicle (n = 15) or Torin1 (20 mg/kg daily, i.p., for 3 days; n = 7) normalized to control tumor. Treatment was started 10 days after tumor initiation. The mice were sacrificed 2 h after the last dose of Torin1. Bar graphs are presented as mean ± SD from biological independent samples. Statistical testing was performed by a two-sided unpaired Student's t test.

(B) Sapienate to palmitate ratio in HUH7 orthotopic liver xenografts treated with vehicle (n = 24) or Torin1 (20 mg/kg daily, i.p., for 3 days; n = 6) normalized to control tumor. Treatment was started 10 days after tumor initiation. The mice were sacrificed 2 h after the last dose of Torin1. Bar graphs are presented as mean ± SD from biological independent samples. Statistical testing was performed by a two-sided unpaired Student's t test.

Inhibiting mTOR Signaling Reduces FADS2 Expression and Sapienate Metabolism *In Vivo*

Finally, we assessed sapienate metabolism *in vivo* in HUH7 orthotopic liver xenografts upon mTOR inhibition. Specifically, we implanted HUH7 cancer cells in the liver of NMRI$^{nu/nu}$ mice and treated the mice after tumor development with three doses of Torin1 (20 mg per kg, daily, intraperitoneal [i.p.]). Subsequently, we measured *FADS2* mRNA expression and the ratio of sapienate to palmitate in tumor tissue of control and Torin1-treated animals. In line with our *in vitro* data, we found that acute mTOR inhibition with Torin1 reduced *FADS2* expression and the sapienate to palmitate ratio in HUH7 tumor tissue (Figures 5A and 5B). Thus, we conclude that mTOR can also regulate *FADS2* expression and sapienate metabolism *in vivo*.

Taken together, we conclude that mTOR signaling or SREBP activity is sufficient to modulate sapienate metabolism in transformed cells and tumor tissue.

DISCUSSION

mTOR and SREBPs are known regulators of lipid metabolism (Mossmann et al., 2018). Here, we identify FADS2 and sapienate metabolism as targets of mTOR and SREBP signaling in mouse and human (cancer) cells. Similar to the well-characterized desaturase SCD1, FADS2 mRNA and protein expression can be modulated through mTOR signaling and is a target of SREBP-1 and SREBP-2. This is in agreement with previous research (Griffiths et al., 2013; Lewis et al., 2015) and suggests that sapienate metabolism is coordinated in line with palmitoleate metabolism. This could explain our observation that many cancer cells competent in sapienate metabolism use sapienate and palmitoleate metabolism simultaneously (Vriens et al., 2019).

We find that in Tsc2 wild-type MEFs, rapamycin and Torin1 are not sufficient to decrease sapienate metabolism, while SREBP inhibition effectively decreased it. This suggests, that in nontransformed (MEF) cells, SREBP controls sapienate biosynthesis independently of mTOR signaling. This is in line with literature indicating that SREBP activity can be altered by sirtuin 1 (Ponugoti et al., 2010), O-GlcNAc transferase (Sodi et al., 2018), and polyunsaturated fatty acids (Worgall et al., 1998). Interestingly, FADS2 is also known to be involved in the polyunsaturation of the essential fatty acid linoleate (Stoffel et al., 2008; Tosi et al., 2014), which results in arachidonate biosynthesis. In this respect, it has been found that silencing of elongation of very-long-chain fatty acids protein 2 (ELOVL2), which functions in conjunction with FADS2 in linoleate metabolism, is detrimental to glioblastoma cells (Gimple et al., 2019). Accordingly, we find that in glioblastoma *FADS2* mRNA expression is highly correlated with mTOR activity (Figure 1A). Thus, based on the data presented here, we would expect that also sapienate metabolism is increased in glioblastomas. Moreover, in genetically engineered *FADS2*-overexpressing cancer cells, it has been found that shifting the ratio between palmitate and linoleate in favor of palmitate can drive sapienate biosynthesis (Park et al., 2016). While we have found

(C and F) Relative sapienate (C) and palmitoleate (F) levels in U87 cells stably expressing ER-mSREBP-1 or ER-mSREBP-2 (n = 3). Bar graphs are presented as mean ± SD from biological independent samples. Statistical testing was performed by a two-sided unpaired Student's t test.

(G) Relative *FADS2* mRNA expression upon treatment with DMSO (n = 10) or fatostatin (10 μM, 72 h, WT n = 11, Tsc2$^{-/-}$ n = 10, HUH7 n = 9) in WT and Tsc2$^{-/-}$ MEFs or HUH7 cancer cells. Bar graphs are presented as mean ± SD from biological independent samples. Statistical testing was performed by a two-sided unpaired Student's t test.

(H) Sapienate to palmitate ratio upon treatment with DMSO (n = 12) or fatostatin (10 μM, 72 h, MEFs n = 12, HUH7 n = 11) in WT and Tsc2$^{-/-}$ MEFs or HUH7 cancer cells. Bar graphs are presented as mean ± SD from biological independent samples. Statistical testing was performed by a two-sided unpaired Student's t test.

(I) Relative sapienate level upon treatment with DMSO (n = 12) or fatostatin (10 μM, 72 h, MEFs n = 12, HUH7 n = 11) in WT and Tsc2$^{-/-}$ MEFs or HUH7 cancer cells. Bar graphs are presented as mean ± SD from biological independent samples. Statistical testing was performed by a two-sided unpaired Student's t test.

(J and M) Relative FADS2 (J) and SCD1 (M) protein expression upon treatment with DMSO or fatostatin (10 μM, 72 h, n = 3) in HUH7 cancer cells. Bar graphs are presented as mean ± SD from biological independent samples. Statistical testing was performed by a two-sided unpaired Student's t test.

(K) Relative *SCD1* mRNA expression in WT and Tsc2$^{-/-}$ MEFs or HUH7 cancer cells upon treatment with DMSO (MEFs n = 6, HUH7 n = 11) or fatostatin (10 μM, 72 h, MEFs n = 7, HUH7 n = 9). Bar graphs are presented as mean ± SD from biological independent samples. Statistical testing was performed by a two-sided unpaired Student's t test.

(L) Palmitoleate to palmitate ratio in WT and Tsc2$^{-/-}$ MEFs or in HUH7 cancer cells upon treatment with DMSO (n = 12) or fatostatin (10 μM, 72 h, MEFs n = 12, HUH7 n = 11). Bar graphs are presented as mean ± SD from biological independent samples. Statistical testing was performed by a two-sided unpaired Student's t test.

previously that linoleate metabolism is not altered by *FADS2* silencing, we have seen that linoleate abundance is decreased in HUH7 tumor tissue compared to adjacent liver tissue (Vriens et al., 2019). This microenvironmental alteration is in line with emerging evidence that nutrient availability in tumor tissue is selectively different compared to healthy compartments (Sullivan et al., 2019). Accordingly, it has been found that nutrient availability is an important metabolic regulator of cancer cell metabolism (Elia and Fendt, 2016; Elia et al., 2019). Thus, it is tempting to speculate that altering linoleate abundance could result in the regulation of sapienate metabolism independently of gene expression in tumors.

In conclusion, we find that sapienate metabolism can be regulated by mTOR and SREBPs in cancer cells, which can explain the dual activity of sapienate and palmitoleate metabolism in most cancers with plasticity in their fatty acid desaturation.

STAR★METHODS

Detailed methods are provided in the online version of this paper and include the following:

- KEY RESOURCES TABLE
- RESOURCE AVAILABILITY
  - Lead Contact
  - Materials Availability
  - Data and Code Availability
- EXPERIMENTAL MODEL AND SUBJECT DETAILS
  - Cell lines
  - Mice
- METHOD DETAILS
  - Reagents and chemicals
  - Generation of inducible SREBP constructs
  - RNA isolation and quantitative real-time PCR
  - Chromatin Immunoprecipitation (ChIP)
  - Western blot analysis
  - Labeling experiments
  - Metabolite extraction
  - GC-MS acquisition and metabolite measurement
  - FADS2 protein analysis
  - Bioinformatic analysis
  - Orthotopic HUH7 xenograft mouse model
- QUANTIFICATION AND STATISTICAL ANALYSIS

SUPPLEMENTAL INFORMATION

Supplemental Information can be found online at https://doi.org/10.1016/j.celrep.2020.107806.

ACKNOWLEDGMENTS

We would like to thank J. Blenis (Cornell Medical) for the kind gift of MEFs cells and J.V. Swinnen (KU Leuven) for providing fatostatin, F. Impens and S. Dufour (VIB Proteomics Core) for performing the protein analysis, and V. van Hoef (VIB-CCB Bioinformatics Expertise Center) for part of the bioinformatic analysis of TCGA data (https://www.cancer.gov/about-nci/organization/ccg/research/structural-genomics/tcga). For funding, G.R. has received consecutive PhD fellowships from Kom op tegen Kanker and FWO. A.S., S.J.R., A.M.W., and C.R.M. acknowledge funding by the German Research Foundation (GRK2243 and SCHU-2670/1). The laboratory of T.G.P.G. is supported by grants from the German Cancer Aid (DKH-70112257), the Gert and Susanna Mayer Foundation, and the Barbara and Wilfried Mohr Foundation. S.-M.F. acknowledges funding from the European Research Council under ERC consolidator grant 771486–MetaRegulation, Marie Curie CIG n.617727–Metabolism-Connect, FWO research projects (G098120N), FWO Odysseus II, and KU Leuven Methusalem co-funding.

AUTHOR CONTRIBUTIONS

M.T. conducted the experiments and coordinated the project. G.R., M.P., and A.V. performed and analyzed the labeling experiments. G.R. performed the WB, expression, and metabolite measurement of U87 cells. A.S. contributed to the generation of the SREBP results. A.M.W., C.R.M., and S.J.R. generated the ChIP-qPCR data and SREBP expression data. M.T., D.B., and J.V.E. performed mouse experiments. M.F.O. and T.G.P.G. provided the bioinformatic analysis for the survival data. M.T. and G.R. acquired, analyzed, and interpreted the data. M.T. and S.-M.F. designed the study. S.-M.F. wrote the original draft, which was reviewed and edited by M.T. S.-M.F. conceived and supervised the study. All authors read and approved the final manuscript.

DECLARATION OF INTERESTS

S.-M.F. has received funding from Bayer, Merck, and Black Belt Therapeutics and has consulted for Funds+.

Received: October 28, 2019
Revised: April 3, 2020
Accepted: June 2, 2020
Published: June 23, 2020

REFERENCES

Baluapuri, A., Hofstetter, J., Dudvarski Stankovic, N., Endres, T., Bhandare, P., Vos, S.M., Adhikari, B., Schwarz, J.D., Narain, A., Vogt, M., et al. (2019). MYC recruits SPT5 to RNA polymerase II to promote processive transcription elongation. Mol. Cell *74*, 674–687.e11.

Ben-Sahra, I., and Manning, B.D. (2017). mTORC1 signaling and the metabolic control of cell growth. Curr. Opin. Cell Biol. *45*, 72–82.

Buescher, J.M., Antoniewicz, M.R., Boros, L.G., Burgess, S.C., Brunengraber, H., Clish, C.B., DeBerardinis, R.J., Feron, O., Frezza, C., Ghesquiere, B., et al. (2015). A roadmap for interpreting (13)C metabolite labeling patterns from cells. Curr. Opin. Biotechnol. *34*, 189–201.

Cheng, X., Li, J., and Guo, D. (2018). SCAP/SREBPs are central players in lipid metabolism and novel metabolic targets in cancer therapy. Curr. Top. Med. Chem. *18*, 484–493.

Cho, H.P., Nakamura, M.T., and Clarke, S.D. (1999). Cloning, expression, and nutritional regulation of the mammalian Δ-6 desaturase. J. Biol. Chem. *274*, 471–477.

Christen, S., Lorendeau, D., Schmieder, R., Broekaert, D., Metzger, K., Veys, K., Elia, I., Buescher, J.M., Orth, M.F., Davidson, S.M., et al. (2016). Breast cancer-derived lung metastasis show increased pyruvate carboxylase-dependent anaplerosis. Cell Rep. *17*, 837–848.

Currie, E., Schulze, A., Zechner, R., Walther, T.C., and Farese, R.V., Jr. (2013). Cellular fatty acid metabolism and cancer. Cell Metab. *18*, 153–161.

Dong, X., Tan, P., Cai, Z., Xu, H., Li, J., Ren, W., Xu, H., Zuo, R., Zhou, J., Mai, K., and Ai, Q. (2017). Regulation of FADS2 transcription by SREBP-1 and PPAR-α influences LC-PUFA biosynthesis in fish. Sci. Rep. *7*, 40024.

Eid, W., Dauner, K., Courtney, K.C., Gagnon, A., Parks, R.J., Sorisky, A., and Zha, X. (2017). mTORC1 activates SREBP-2 by suppressing cholesterol trafficking to lysosomes in mammalian cells. Proc. Natl. Acad. Sci. USA *114*, 7999–8004.

Elia, I., and Fendt, S.-M. (2016). In vivo cancer metabolism is defined by the nutrient microenvironment. Transl. Cancer Res. *5*, S1284–S1287.

Elia, I., Rossi, M., Stegen, S., Broekaert, D., Doglioni, G., van Gorsel, M., Boon, R., Escalona-Noguero, C., Torrekens, S., Verfaillie, C., et al. (2019). Breast

cancer cells rely on environmental pyruvate to shape the metastatic niche. Nature *568*, 117–121.

Gimple, R.C., Kidwell, R.L., Kim, L.J.Y., Sun, T., Gromovsky, A.D., Wu, Q., Wolf, M., Lv, D., Bhargava, S., Jiang, L., et al. (2019). Glioma stem cell-specific superenhancer promotes polyunsaturated fatty-acid synthesis to support EGFR signaling. Cancer Discov. *9*, 1248–1267.

Griffiths, B., Lewis, C.A., Bensaad, K., Ros, S., Zhang, Q., Ferber, E.C., Konisti, S., Peck, B., Miess, H., East, P., et al. (2013). Sterol regulatory element binding protein-dependent regulation of lipid synthesis supports cell survival and tumor growth. Cancer Metab. *1*, 3–3.

Han, J., Li, E., Chen, L., Zhang, Y., Wei, F., Liu, J., Deng, H., and Wang, Y. (2015). The CREB coactivator CRTC2 controls hepatic lipid metabolism by regulating SREBP1. Nature *524*, 243–246.

Hanahan, D., and Weinberg, R.A. (2011). Hallmarks of cancer: the next generation. Cell *144*, 646–674.

Kharroubi, A.T., Masterson, T.M., Aldaghlas, T.A., Kennedy, K.A., and Kelleher, J.K. (1992). Isotopomer spectral analysis of triglyceride fatty acid synthesis in 3T3-L1 cells. Am. J. Physiol. *263*, E667–E675.

Laplante, M., and Sabatini, D.M. (2009). An emerging role of mTOR in lipid biosynthesis. Curr. Biol. *19*, R1046–R1052.

Laplante, M., and Sabatini, D.M. (2012). mTOR signaling in growth control and disease. Cell *149*, 274–293.

Lêthibichthuy, Ciorbaru, R., and Brochier, J. (1978). Human B cell differentiation. I. Immunoglobulin synthesis induced by Nocardia mitogen. Eur. J. Immunol. *8*, 119–123.

Lewis, C.A., Brault, C., Peck, B., Bensaad, K., Griffiths, B., Mitter, R., Chakravarty, P., East, P., Dankworth, B., Alibhai, D., et al. (2015). SREBP maintains lipid biosynthesis and viability of cancer cells under lipid- and oxygen-deprived conditions and defines a gene signature associated with poor survival in glioblastoma multiforme. Oncogene *34*, 5128–5140.

Liu, Q., Chang, J.W., Wang, J., Kang, S.A., Thoreen, C.C., Markhard, A., Hur, W., Zhang, J., Sim, T., Sabatini, D.M., and Gray, N.S. (2010). Discovery of 1-(4-(4-propionylpiperazin-1-yl)-3-(trifluoromethyl)phenyl)-9-(quinolin-3-yl)benzo[h][1,6]naphthyridin-2(1H)-one as a highly potent, selective mammalian target of rapamycin (mTOR) inhibitor for the treatment of cancer. J. Med. Chem. *53*, 7146–7155.

Liu, Q., Kang, S.A., Thoreen, C.C., Hur, W., Wang, J., Chang, J.W., Markhard, A., Zhang, J., Sim, T., Sabatini, D.M., and Gray, N.S. (2012). Development of ATP-competitive mTOR inhibitors. Methods Mol. Biol. *821*, 447–460.

Lorendeau, D., Christen, S., Rinaldi, G., and Fendt, S.-M. (2015). Metabolic control of signalling pathways and metabolic auto-regulation. Biol. Cell *107*, 251–272.

Lorendeau, D., Rinaldi, G., Boon, R., Spincemaille, P., Metzger, K., Jäger, C., Christen, S., Dong, X., Kuenen, S., Voordeckers, K., et al. (2017). Dual loss of succinate dehydrogenase (SDH) and complex I activity is necessary to recapitulate the metabolic phenotype of SDH mutant tumors. Metab. Eng. *43*, 187–197.

Madison, B.B. (2016). Srebp2: A master regulator of sterol and fatty acid synthesis. J. Lipid Res. *57*, 333–335.

Manning, B.D., and Cantley, L.C. (2003). United at last: the tuberous sclerosis complex gene products connect the phosphoinositide 3-kinase/Akt pathway to mammalian target of rapamycin (mTOR) signalling. Biochem. Soc. Trans. *31*, 573–578.

Matsuzaka, T., Shimano, H., Yahagi, N., Amemiya-Kudo, M., Yoshikawa, T., Hasty, A.H., Tamura, Y., Osuga, J., Okazaki, H., Iizuka, Y., et al. (2002). Dual regulation of mouse Δ(5)- and Δ(6)-desaturase gene expression by SREBP-1 and PPARalpha. J. Lipid Res. *43*, 107–114.

Mossmann, D., Park, S., and Hall, M.N. (2018). mTOR signalling and cellular metabolism are mutual determinants in cancer. Nat. Rev. Cancer *18*, 744–757.

Park, H.G., Kothapalli, K.S.D., Park, W.J., DeAllie, C., Liu, L., Liang, A., Lawrence, P., and Brenna, J.T. (2016). Palmitic acid (16:0) competes with omega-6 linoleic and omega-3 α-linolenic acids for FADS2 mediated Δ6-desaturation. Biochim. Biophys. Acta *1861*, 91–97.

Peck, B., and Schulze, A. (2016). Lipid desaturation - the next step in targeting lipogenesis in cancer? FEBS J. *283*, 2767–2778.

Peck, B., Schug, Z.T., Zhang, Q., Dankworth, B., Jones, D.T., Smethurst, E., Patel, R., Mason, S., Jiang, M., Saunders, R., et al. (2016). Inhibition of fatty acid desaturation is detrimental to cancer cell survival in metabolically compromised environments. Cancer Metab. *4*, 6.

Ponugoti, B., Kim, D.-H., Xiao, Z., Smith, Z., Miao, J., Zang, M., Wu, S.-Y., Chiang, C.-M., Veenstra, T.D., and Kemper, J.K. (2010). SIRT1 deacetylates and inhibits SREBP-1C activity in regulation of hepatic lipid metabolism. J. Biol. Chem. *285*, 33959–33970.

Porstmann, T., Santos, C.R., Griffiths, B., Cully, M., Wu, M., Leevers, S., Griffiths, J.R., Chung, Y.-L., and Schulze, A. (2008). SREBP activity is regulated by mTORC1 and contributes to Akt-dependent cell growth. Cell Metab. *8*, 224–236.

Röhrig, F., and Schulze, A. (2016). The multifaceted roles of fatty acid synthesis in cancer. Nat. Rev. Cancer *16*, 732–749.

Saxton, R.A., and Sabatini, D.M. (2017). mTOR signaling in growth, metabolism, and disease. Cell *168*, 960–976.

Sodi, V.L., Bacigalupa, Z.A., Ferrer, C.M., Lee, J.V., Gocal, W.A., Mukhopadhyay, D., Wellen, K.E., Ivan, M., and Reginato, M.J. (2018). Nutrient sensor O-GlcNAc transferase controls cancer lipid metabolism via SREBP-1 regulation. Oncogene *37*, 924–934.

Stoffel, W., Holz, B., Jenke, B., Binczek, E., Günter, R.H., Kiss, C., Karakesisoglou, I., Thevis, M., Weber, A.-A., Arnhold, S., and Addicks, K. (2008). Delta6-desaturase (FADS2) deficiency unveils the role of omega3- and omega6-polyunsaturated fatty acids. EMBO J. *27*, 2281–2292.

Sullivan, M.R., Danai, L.V., Lewis, C.A., Chan, S.H., Gui, D.Y., Kunchok, T., Dennstedt, E.A., Vander Heiden, M.G., and Muir, A. (2019). Quantification of microenvironmental metabolites in murine cancers reveals determinants of tumor nutrient availability. eLife *8*, e44235.

Tosi, F.S.F., Guarini, P., Olivieri, O., and Martinelli, N. (2014). Delta-5 and Delta-6 desaturases: crucial enzymes in polyunsaturated fatty acid-related pathways with pleiotropic influences in health and disease. In Oxidative Stress and Inflammation in Non-communicable Diseases: Molecular Mechanisms and Perspectives in Therapeutics. Advances in Experimental Medicine and Biology, J. Camps, ed. (Springer), pp. 66–81.

Vivian, J., Rao, A.A., Nothaft, F.A., Ketchum, C., Armstrong, J., Novak, A., Pfeil, J., Narkizian, J., Deran, A.D., Musselman-Brown, A., et al. (2017). Toil enables reproducible, open source, big biomedical data analyses. Nat. Biotechnol. *35*, 314–316.

Vriens, K., Christen, S., Parik, S., Broekaert, D., Yoshinaga, K., Talebi, A., Dehairs, J., Escalona-Noguero, C., Schmieder, R., Cornfield, T., et al. (2019). Evidence for an alternative fatty acid desaturation pathway increasing cancer plasticity. Nature *566*, 403–406.

Wong, M. (2010). Mammalian target of rapamycin (mTOR) inhibition as a potential antiepileptogenic therapy: From tuberous sclerosis to common acquired epilepsies. Epilepsia *51*, 27–36.

Worgall, T.S., Sturley, S.L., Seo, T., Osborne, T.F., and Deckelbaum, R.J. (1998). Polyunsaturated fatty acids decrease expression of promoters with sterol regulatory elements by decreasing levels of mature sterol regulatory element-binding protein. J. Biol. Chem. *273*, 25537–25540.

Yoo, H., Stephanopoulos, G., and Kelleher, J.K. (2004). Quantifying carbon sources for de novo lipogenesis in wild-type and IRS-1 knockout brown adipocytes. J. Lipid Res. *45*, 1324–1332.

Zhang, Y., Kwok-Shing Ng, P., Kucherlapati, M., Chen, F., Liu, Y., Tsang, Y.H., de Velasco, G., Jeong, K.J., Akbani, R., Hadjipanayis, A., et al. (2017). A Pan-Cancer Proteogenomic Atlas of PI3K/AKT/mTOR Pathway Alterations. Cancer Cell *31*, 820–832.e3.

Zheng, Y., and Jiang, Y. (2015). mTOR Inhibitors at a Glance. Mol. Cell. Pharmacol. *7*, 15–20.

STAR★METHODS

KEY RESOURCES TABLE

REAGENT or RESOURCE	SOURCE	IDENTIFIER
Antibodies		
Rabbit monoclonal anti-pS6K1(Thr389)	Cell Signaling Technology	Cat# 9205, RRID:AB_330944
Rabbit monoclonal anti-S6K1	Cell Signaling Technology	Cat# 9202, RRID:AB_331676
Rabbit monoclonal anti-pS6(S240/S244)	Cell Signaling Technology	Cat# 2215, RRID:AB_331682
Rabbit monoclonal anti-S6	Cell Signaling Technology	Cat# 2217, RRID:AB_331355
Rabbit monoclonal anti-4E-BP1	Cell Signaling Technology	Cat# 9452, RRID:AB_331692
Mouse monoclonal anti-Actin	Sigma-Aldrich	Cat# A5441, RRID:AB_476744
Anti-mouse IgG, HRP-linked Antibody	Cell Signaling Technology	Cat# 7076, RRID:AB_330924
Anti-rabbit IgG, HRP-linked Antibody	Cell Signaling Technology	Cat# 7074, RRID:AB_2099233
Anti-SREBP-1 (2A4)	In-house prepared from ATCC hybridoma	Cat# CRL-2121 RRID:CVCL_G659
Anti-SREBP–2 (1D2)	In-house prepared from ATCC hybridoma	Cat# CRL-2545 RRID:CVCL_G658
Anti-SREB-1 (H160-X)	Santa Cruz	No longer available
Anti-IgG	Sigma-Aldrich	Cat# I5006 RRID:AB_1163659
Chemicals, Peptides, and Recombinant Proteins		
Rapamycin	Bio Connect	Cat# 53123-88-9
Torin1	Bio Connect	Cat# 1222998-36-8
Fatostatin	Tocris Bioscience	Cat# 4444
4-Hydroxytamoxifen	Sigma-Aldrich	Cat# H7904
Chloroform	Sigma-Aldrich	Cas# 67-66-3
Methanol	Sigma-Aldrich	Cas# 67-56-1
Hexane	Sigma-Aldrich	Cas# 110-54-3
Sulfuric acid	Sigma-Aldrich	Cas# 7664-93-9
Pentadecanoic acid (C15:0)	Sigma-Aldrich	Cas# 1002-84-2
Heptadecanoic acid (C17:0)	Sigma-Aldrich	Cas# 506-12-7
RIPA	Thermo Fisher Scientific	Cat# 89901
Critical Commercial Assays		
TRIzol Reagent	Thermo Fisher	Cat# 15596026
Qscript cDNA synthesis kit	Quantabio	Cat# 95047-500
SYBR Green Master Mix	Thermo Fisher Scientific	Cat# 4309155
Platinum SYBR Green qPCR SuperMix	Life technologies	Cat# 11744100
Power up Master Mix	Thermo Fisher Scientific	Cat# A25778
Protease inhibitor	Roche	Cat# 11836153001
PhosSTOP	Sigma-Aldrich	Cat# 4906845001
BCA protein assay kit	Thermo Fisher Scientific	Cat# 23227
SuperSignal West Femto Maximum Sensitivity Substrate	Thermo Fisher Scientific	Cat# 34095
Experimental Models: Cell Lines		
WT and $Tsc2^{-/-}$ MEFs	provided by Dr. John Blenis	N/A
HUH7 hepato cellular carcinoma	JCRB	Cat# JCRB0403, RRID:CVCL_0336
U87 MG glioblastoma cells	provided by Prof. Adrian Harris	N/A
U2OS osteosarcoma cells	provided by CRUK London Research Institute Cell Services	N/A

(*Continued on next page*)

Continued

REAGENT or RESOURCE	SOURCE	IDENTIFIER
Experimental Models: Organisms/Strains		
Male immunocompromised NMRI$^{nu/nu}$ mice	Taconic M&B AS, Ejby, Denmark	Model# NMRINU-M
Oligonucleotides		
FADS2_ChIP site A_Fw: 5′-TCTGCTGATCGCTGTGGAAACT-3′	Sigma-Aldrich	N/D
FADS2_ChIP site_Rv: 5′-TCTGCTGATCGCTGTGGAAACT-3′	Sigma-Aldrich	N/D
FADS2_ChIP site B_Fw: 5′-TGGAGGCAAAAGTCCATAGC-3′	Sigma-Aldrich	N/D
FADS2_ChIP site B_Rv: 5′-GATCCCTGGCTTCCCAGT-3′	Sigma-Aldrich	N/D
Primers for RT-qPCR, See Table S5	This paper	N/D
Recombinant DNA		
ER-mSREBP-1	provided by Dr. Almut Schulze	Lewis et al., 2015
ER-mSREBP-2	provided by Dr. Almut Schulze	Lewis et al., 2015
Software and Algorithms		
Prism v.7.0	GraphPad	https://www.graphpad.com/
MATLAB	N/D	https://fr.mathworks.com/
TCGA Database	Open source	https://xena.ucsc.edu/
MaxQuant	PMID 24942700	https://www.maxquant.org/

RESOURCE AVAILABILITY

Lead Contact

Further requests for resources should be directed to the lead contact, Sarah-Maria Fendt (sarah-maria.fendt@kuleuven.vib.be).

Materials Availability

This study did not generate new unique reagents, except of genetically manipulated cell lines based on commercially available constructs. Reagents generated in this study will be made available on request through the lead author or the collaboration partner that generated the resource, but we may require a payment and/or a completed Materials Transfer Agreement if there is potential for commercial application.

Data and Code Availability

The published article includes all analyzed data. The mass spectrometry files supporting the current study have not been deposited in a public repository due to the lack of a commonly accepted and feasible metabolomics file repository but are available upon reasonable request from the lead contact.

EXPERIMENTAL MODEL AND SUBJECT DETAILS

Cell lines

Wild-type and null Tsc2-p53$^{-/-}$ (Tsc2$^{-/-}$) MEFs were kindly provided by Dr John Blenis (Cornell Medical). HUH7 hepato cellular carcinoma cell line was obtained from the Japanese Collection of Research Bioresources (JCRB) Cell Bank (Osaka, Japan). MEFs and HUH7 cells were cultured in high glucose (4.5 g per L) Dulbecco's modified Eagle's medium (DMEM) (Life Technologies, CA, USA) supplemented with 10% heat-inactivated fetal bovine serum (Invitrogen, MA, USA), 1% penicillin (50U per mL) (Life Technologies, CA, USA) and 1% Penicillin-Streptomycin (15 μg per mL) (Life Technologies, CA, USA). Glioblastoma (U87) and osteosarcoma (U2OS) cells were cultured in Dulbecco's Modified Eagle's Medium with high glucose (4.5 g per l) and sodium pyruvate, supplemented with 4 mM L-glutamine (200mM), 1% penicillin/streptomycin (100X) and 10% fetal bovine serum (all Sigma-Aldrich). All cell lines were used at low passage and regularly checked for absence of mycoplasma based on the MycoAlert^{TM} Mycoplasma Detection Kit (Lonza, Basel, Switzerland).

Mice

All animal work was performed in accordance with protocols approved by the Institutional Animal Care and Research Advisory Committee of the KU Leuven, Belgium. 6-week-old male immunocompromised NMRI$^{nu/nu}$ mice (Taconic M&B AS, Ejby, Denmark) were used in this study.

METHOD DETAILS

Reagents and chemicals

mTORC1 inhibitor Rapamycin (53123-88-9) and mTORC1/C2 inhibitor Torin1 (1222998-36-8) were purchased from Bio Connect. SREBP inhibitor Fatostatin (4444) was purchase from Tocris Bioscience. All compounds were dissolved in DMSO and used at the following concentrations: Rapamycin (20 nM), Torin1 (40 nM) and fatostatin (10 μM). All the compounds were added at day 0 and analyzed at day 3. All experiments were performed in $n \geq 3$ biological replicates.

Solvents for metabolite extraction and mass spectrometry were HPLC grade from Sigma-Aldrich (MO, USA). For more info see Key Resources Table.

Generation of inducible SREBP constructs

U87 cells expressing ER-mSREBP-1 or ER-mSREBP-2 were described before (Lewis et al., 2015). Briefly, sequences corresponding to amino acids 2–460 of human SREBP-1a or amino acids 2–468 of human SREBP-2 were fused to the C terminus of the hormone-binding domain of the murine ER (Lêthibichthuy et al., 1978) via a 19-bp linker and cloned into pBabe-puro. Constructs were validated by sequencing and stably expressed in U87-GFP cells using retroviral transduction. U87 cells expressing ER-mSREBP-1 or ER-mSREBP-2 were treated with 100 nM 4-OHT (Sigma-Aldrich) or solvent for 24 h in medium containing 10% FBS.

RNA isolation and quantitative real-time PCR

Total RNA was isolated using TRIzol according to the manufacturer's instruction (Thermo Scientific). cDNA synthesis was performed using 1 μg of RNA with the Qscript cDNA synthesis kit (Quantabio). Gene expression was assessed by quantitative real time PCR using Platinum SYBR Green qPCR SuperMix (Life technologies) and specific primers on a 7500 Fast Real Time PCR System (Applied Biosystems, Life technologies) or by using PowerUp SYBR® Green Master Mix and respective primers on a StepOnePlus Real-Time PCR System (Applied Biosystems). Amplification was performed at 95°C for 10 min, followed by 40 cycles of 15 s at 95°C and 1 min at 60°C. Samples were assayed in triplicates. All gene expression was normalized to the *RPL19* or *ACTB* housekeeper genes. Primer sequences are listed in Table S5.

Chromatin Immunoprecipitation (ChIP)

ChIP experiments were performed as previously described (Baluapuri et al., 2019) using 30 μg anti-SREBP-1 (IgG-2A4, CRL-21212A4) or anti-SREBP-2 (IgG-1D2 CRL-2545) (both isolated from hybridoma cells obtained from ATCC) or using Anti-SREBP-1 (H160-X) (Santa Cruz). Chromatin was analyzed by qPCR using StepOnePlus Real-Time PCR System (Thermo Fisher Scientific) and SYBR Green Master Mix (Thermo Fisher Scientific). Primer sequences for FADS2 (Site A) and FADS2 (Site B) are listed in Table S5.

Western blot analysis

Cells were collected and then lysed in RIPA lysis and extraction buffer (Thermo Scientific) supplemented with protease inhibitor (Roche, 11836153001) and phosphatase (PhosSTOP, Sigma, 4906845001). Protein concentration was measured using the pierce BCA protein assay kit (Thermo Scientific). 30μg of protein were loaded on a NuPAGE 4%–12% denaturing Bis-Tris gel and transferred to a nitrocellulose membrane (Thermo Scientific). Membranes were blocked in non-fat dry milk and incubated overnight at 4°C with either pS6K1 (Cell Signaling Technology, 9205; 1:1,000 dilution), S6K1 (Cell Signaling Technology, 9202; 1:1,000 dilution), pS6 (Cell Signaling Technology, 2215; 1:1,000 dilution), S6 (Cell Signaling Technology, 2217; 1:1,000 dilution), 4EBP1 (Cell Signaling Technology, 9452; 1:1,000 dilution) or β-Actin (Sigma, A5441; 1:10,000 dilution) primary antibodies. The day after the membranes were incubated with either mouse (Cell Signaling Technology, 7076; 1:2,000 dilution) or with rabbit (Cell Signaling Technology, 7074; 1:2,000 dilution) secondary antibodies. The signal was visualized using the Pierce SuperSignal West Pico Plus Chemiluminescent Substrate (Thermo Scientific).

Labeling experiments

Cells were seeded in the wells of 6-well plates (Corning, NY, USA) at either $1,5 \times 10^4$ cells per well (MEF wild-type and Tsc2$^{-/-}$) or 6×10^4 cells per well (HUH7) and grown in a humidified environment at 37 °C with 5% CO_2. After 24 h, the medium was aspirated, cells were washed with DPBS and DMEM (4.5 g per l $^{13}C_6$-glucose, 10% dialyzed FBS, 1% Penicillin/Streptomycin) supplemented with 0.1% DMSO (control) or Torin1 (40 nM) was added to the wells (3 mL per well). After 72 h of incubation, cells were washed with saline solution (NaCl 0.9%) after treatment and metabolism was quenched by flash-freezing the plates in liquid nitrogen. Plates were stored at –80 °C until metabolite extraction. All experiments were performed in triplicates.

Metabolite extraction

Metabolite extractions were performed using the methods described in Christen et al. (2016) and Lorendeau et al. (2017) Briefly, for cell culture plates containing 100k-500k cells per well, medium was aspirated, cells were washed with blood bank saline and cell metabolism was quenched by flash-freezing the plates in liquid nitrogen. Next, 800 μL of cold 62.5% methanol in water was added to the wells, cells were scraped with a pipet tip and suspensions were transferred to Eppendorf tubes. Next, 500 μL of cold chloroform

was added and samples were vortexed at 4°C for 10 min to extract metabolites. Phase separation was achieved by centrifugation at 4°C for 10 min, after which the chloroform phase (containing the total fatty acid content) was separated and dried by vacuum centrifugation.

For tissue samples, tissues were weighed (5-10 mg) and pulverized (Cryomill, Retsch) under liquid nitrogen conditions. Next, 800 μL cold 62.5% methanol in water was added to the samples, followed by 500 μL cold chloroform. Samples were then handled as described above. Dried fatty acid samples were immediately processed to fatty acid methyl esters as described below, thereby avoiding degradation.

Total fatty acid samples were esterified with 500 μL 2% sulfuric acid in methanol for 3h at 60°C or overnight at 50°C (for tissue samples) and extracted by addition of 600 μL hexane and 100 μL saturated NaCl. Samples were centrifuged for 5 min and the hexane phase was separated and dried by vacuum centrifugation and resuspended in hexane.

GC-MS acquisition and metabolite measurement

Isotopologue distributions of fatty acids were measured with gas chromatography (7890A GC system, Agilent Technologies, CA, USA) combined with mass spectrometry (5975C Inert MS system, Agilent Technologies, CA, USA). One microliter of each sample was injected a split ratio 1 to 3 mode with an inlet temperature of 270°C onto a DB35MS column. Helium was used as a carrier gas with a flowrate of 1 mL min-1. To ensure the separation of fatty acids, the initial gradient temperature was set at 140°C for 2 min and increased at the ramping rate of 1°C/min to 185°C, following by a ramping rate of 20°C/min to rich 300°C. The temperatures of the quadrupole and the source were set at 150°C and 230°C, respectively. For polyunsaturated fatty acids, they were measured with gas chromatography (8860 GC system, Agilent Technologies, CA, USA) combined with mass spectrometry (5977B Inert MS system, Agilent Technologies, CA, USA). One microliter of each sample was injected (splitless mode) with an inlet temperature of 270°C onto a DB-FASTFAME column. Helium was used as a carrier gas with a flow rate of 1 mL/min. For fatty acids separation, the initial gradient temperature was set at 50°C for 1 min then increased at the ramping rate of 12°C/min to 180°C, following by a ramping rate of 1°C/min to rich 200°C. Finally, the final gradient temperature was set at 230°C with a ramping rate of 5°C/min for 2 min. The temperatures of the quadrupole and the source were set at 150°C and 230°C, respectively. The MS system was operated under electron impact ionization at 70eV and a mass range of 100-600 amu was scanned. Isotopologue distributions were extracted from the raw chromatograms using an in-house MATLAB script. Palmitate, palmitoleate and sapienate synthesis were calculated based on isotopologue distributions of the according fatty acid, using Isotopomer Spectral Analysis (ISA)(Kharroubi et al., 1992) and an in-house MATLAB script. For determination of relative metabolite abundances, the total ion counts were normalized to the internal standard (pentadecanoate or heptadecanoate) and the protein content for cell extracts. For tissue extracts, the total ion counts were normalized to the internal standard (pentadecanoate) and tissue weight. The desaturation activity from palmitate to sapienate or palmitoleate was calculated by dividing the normalized total ion count of sapienate or palmitoleate by the normalized total ion count of palmitate.

FADS2 protein analysis

HUH7 cell pellets (5 million cells per pellet) in triplicate were lysed in a urea lysis buffer containing 8 M urea and 20 mM HEPES pH 8.0. The cells were homogenized by sonication on a Diagenode Bioruptor Plus instrument using the following settings: high intensity power output, 10 cycles of 30 s ON/30 s OFF pulses, +4°C water bath. The protein concentration in each lysate was measured by Bradford (Biorad) and aliquots containing 100 μg of protein were used for further analysis. Proteins were first reduced by addition of dichlorodiphenyltrichloroethane (DTT) to a concentration of 5 mM and incubation for 30 minutes at 55°C and then alkylated by addition iodoacetamide (IAA) to a concentration of 10 mM for 15 minutes at room temperature in the dark. Samples were diluted with 20 mM HEPES pH 8.0 to a urea concentration of 4 M and proteins were digested with 1 μg lysyl endopeptidase (Wako) (1/100, w/w) for 4 hours at 37°C. Samples were further diluted with 20 mM HEPES pH 8.0 to a final urea concentration of 2 M and proteins were digested with 1 μg trypsin (Promega) (1/100, w/w) overnight at 37°C. The resulting peptide mixture was purified using OMIX C18 pipette tips (Agilent) and 100 μg of peptides of each sample were dried completely by vacuum drying and stored at −20°C until further use.

Purified peptides were re-dissolved in 20 μl loading solvent A (0.1% TFA in water/ACN (98:2, v/v)) of which approximately 3 μg of peptides was injected for LC-MS/MS analysis on an Ultimate 3000 RSLCnano system in-line connected to a Q Exactive HF mass spectrometer (Thermo). Trapping was performed at 10 μl/min for 4 min in loading solvent A on a 20 mm trapping column (made in-house, 100 μm internal diameter, 5 μm beads, C18 Reprosil-HD, Dr. Maisch, Germany). The peptides were separated on a 200 cm μPAC column with C18-endcapped functionality (Pharmafluidics, Belgium) kept at a constant temperature of 50°C. Peptides were eluted by a non-linear gradient reaching 33% MS solvent B (0.1% FA in water/acetonitrile (2:8, v/v)) in 105 min, 55% MS solvent B in 145 min and 99% MS solvent B in 150 min at a constant flow rate of 300 nl/min, followed by a 10-minutes wash at 99% MS solvent B and re-equilibration with MS solvent A (0.1% FA in water). The mass spectrometer was operated in data-dependent mode, automatically switching between MS and MS/MS acquisition for the 16 most abundant ion peaks per MS spectrum. Full-scan MS spectra (375-1500 m/z) were acquired at a resolution of 60,000 in the Orbitrap analyzer after accumulation to a target value of 3,000,000. The 16 most intense ions above a threshold value of 22,000 were isolated for fragmentation at a normalized collision energy of 28% after filling the trap at a target value of 100,000 for maximum 80 ms. MS/MS spectra (200-2,000 m/z) were acquired at a resolution of 15,000 in the Orbitrap analyzer. Data analysis was performed by MaxQuant (version 1.6.3.4) (PMID 19029910) using the Andromeda search engine with default search settings including a false discovery rate set at 1% on both the peptide and protein

level. Spectra were searched against the human proteins in the Swiss-Prot database (database release version of June 2019 containing 20,431 human protein sequences, downloaded from https://www.uniprot.org). The mass tolerance for precursor and fragment ions was set to 4.5 and 20 ppm, respectively, during the main search. Enzyme specificity was set as C-terminal to arginine and lysine (trypsin), also allowing cleavage at arginine/lysine-proline bonds with a maximum of two missed cleavages. Carbamidomethylation of cysteine residues was set as a fixed modification and variable modifications were set to oxidation of methionine residues (to sulfoxides) and acetylation of protein N-termini. Proteins were quantified by the MaxLFQ algorithm integrated in the MaxQuant software (PMID 24942700). Only proteins with at least one unique or razor peptide were retained for identification, while a minimum ratio count of two unique peptides was required for quantification.

Bioinformatic analysis

Expression data. For the TCGA analyses, TOIL-RSEM normalized count data of the TCGA Pan-Cancer dataset (9185 primary tumor samples belonging to 32 cancer types) were retrieved from UCSC Xena (http://xena.ucsc.edu) (Vivian et al., 2017; Zhang et al., 2017). A signature of SREBP-1 activation was defined for all primary tumors as the geometric mean of *SCD1* and *FASN* expression. For 7407 primary tumors, an mTORC1 pathway signature could be scored based on their RPPA profiles. This signature was defined as the sum of phosphoprotein levels of mTOR, 4E-BP1 (S65, T37/T46, and T70 RPPA features), P70S6K, and S6 (S235/S236 and S240/S244 features) and was previously described in Zhang et al.(Zhang et al., 2017). The Pearson correlation coefficients and significance levels between *FADS2* expression and these signatures were calculated using GraphPad Prism 7 (GraphPad Software Inc., CA, USA).
Mutation data. Mutation data of TCGA data as predicted by the Mutect2 pipeline, average copy number of selected genes and *FADS2* normalized expression data was downloaded from the XenaBrowser (https://xenabrowser.net). For each cancer type, TCGA samples were divided by mutation status of *TP53* and *PIK3CA* in wild-type and mutated (defined as having any type of mutation) and *FADS2* expression was compared between both groups using a t test. Additionally, the Pearson correlation between normalized *FADS2* expression and the average copy number of *MYC* and *PTEN* was calculated per cancer type.
Survival analyses. To correlate *FADS2* expression with survival in cancer, normalized RNASeqV2 mRNA expression data for 28 cancer entities and survival data for the corresponding patients were downloaded from The Cancer Genome Atlas (TCGA) project via the TCGA data portal. Patients were stratified by median *FADS2* expression in those with high and low expression, and significance for differential overall survival of these two groups was assessed with the Mantel-Haenszel test with an in-house bioinformatic tool of the working group of T.G.P.G. Kaplan-Meier plots were generated after manually rechecking the data with GraphPad PRISM.

Orthotopic HUH7 xenograft mouse model

For the *in vivo* experiment, control mice were fed the *ad libitum* a CRM (E) expanded low fat diet (Special Diets Services 801730) or control rat-mouse maintenance diet (Sniff; reference: V1534-000) one week prior to the start of the experiments until sacrificing. For the Torin1 treated mice they were fed control rat-mouse maintenance diet one week prior to the start of the experiments until sacrificing. Next, $0.5x10^6$ HUH7 WT cells were orthotopically injected in 100% MatrigelTM, (BD Biosciences) into the left liver lobe of anesthetized (3% isoflurane, 2% oxygen) 6-week-old male immunocompromised $NMRI^{nu/nu}$ mice (Taconic M&B AS, Ejby, Denmark). For pain relief, mice were given 5 mg per kg carprofen subcutaneous before and after surgery and for the following days. 20 mg/kg Torin1 (Liu et al., 2010), in 20% N-methyl-2-pyrrolidone/40% PEG400/40% water (Liu et al., 2012) or vehicle was delivered by i.p. injection once daily for 3 days after the tumor was established (10 days after cell injection). Two hours after the last treatment, mice were humanely euthanized by an intraperitoneal injection of a 60 mg/ml dolethal solution, the tumor nodule was resected, and blood and healthy liver tissue were sampled. For transcripts, proteomics and metabolomic analysis, half of the tumor nodule and non-tumor tissues were rapidly frozen using a liquid nitrogen cooled Biosqueezer (Biospec Products). Tissues were then weighed and pulverized (Cryomill, Retsch) under liquid nitrogen conditions. The pulverized tissues were extracted for RNA, proteins and GC-MS analysis as described above. Humane endpoints were determined as a tumor size of 1.8 cm^3. Following symptoms were monitored and upon detection of one of the symptoms the animal was euthanized: Loss of ability to ambulate, labored respiration, surgical infection or weight loss over 20 % of initial body weight. Housing and experimental animal procedures were approved by the Institutional Animal Care and Research Advisory Committee of the KU Leuven, Belgium.

QUANTIFICATION AND STATISTICAL ANALYSIS

Statistical data analysis was performed using GraphPad Prism 7 (GraphPad Software Inc., CA, USA) on $n \geq 3$ biological replicates. The statistical methods used and the p values defining significance are stated in all figure legends referencing this data. Detection of mathematical outliers was performed using Grubb's test. Sample size for all experiments was chosen empirically. Data are presented as mean ± SD, as indicated in the figure legends.

Cell Reports, Volume *31*

Supplemental Information

mTOR Signaling and SREBP Activity Increase FADS2 Expression and Can Activate Sapienate Biosynthesis

Mouna Triki, Gianmarco Rinaldi, Melanie Planque, Dorien Broekaert, Alina M. Winkelkotte, Carina R. Maier, Sudha Janaki Raman, Anke Vandekeere, Joke Van Elsen, Martin F. Orth, Thomas G.P. Grünewald, Almut Schulze, and Sarah-Maria Fendt

Supplementary figures and tables

Figure S1

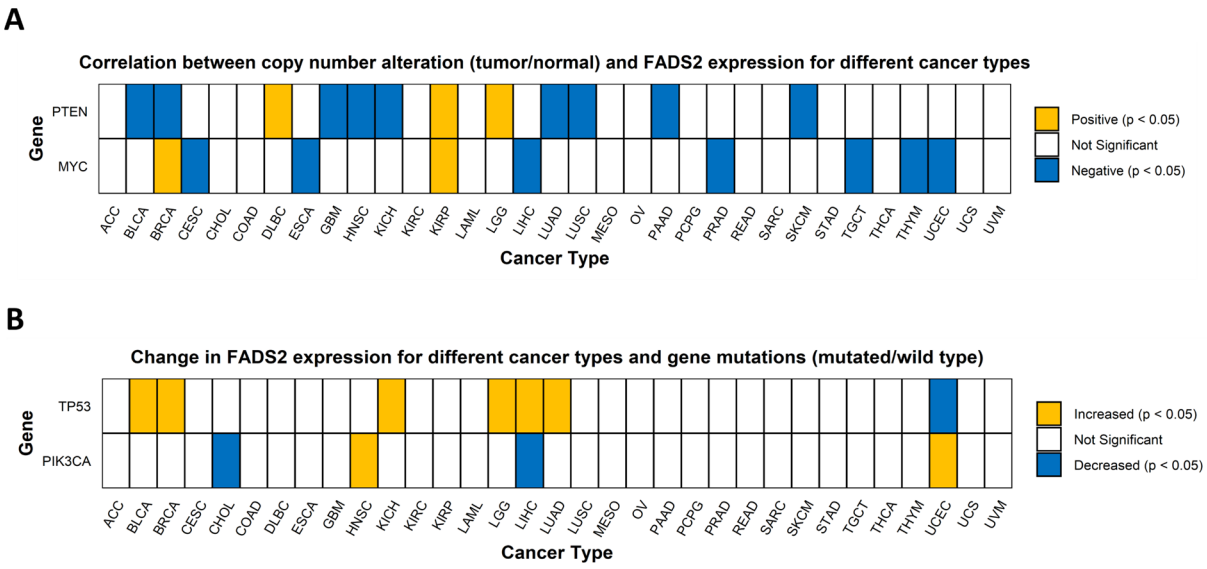

Figure S1: Correlation of *FADS2* expression with copy number and DNA mutations status of signature genes in TCGA database, Related to Figure 1 and Table S4

(A) Heat map representing the correlation between *FADS2* expression and the average copy number alteration of *PTEN* and *MYC* based on the TCGA data derived from 12,650 patients representing 33 major human cancer type. Positive correlations ($p<0.05$) are indicated in yellow and negative correlations ($p<0.05$) are indicated in blue. No significant correlations ($p>0.05$) are presented in white.

(B) Heat map representing the correlation between *FADS2* and the average of *TP53* and *PIK3CA* mutations. TCGA samples representing 33 major human cancer type were divided by mutation status of *TP53* and *PIK3CA* in wild type and mutated (defined as having any type of mutation) and *FADS2* expression was compared between both groups using a t-test. Correlations ($p<0.05$) between increased *FADS2* expression and the presence of mutations are indicated in yellow; correlations ($p<0.05$) between decreased *FADS2* expression and the presence of mutations are indicated in blue. No significant correlations ($p>0.05$) are presented in white.

ACC: Adrenocortical carcinoma, BLCA: Bladder Urothelial Carcinoma, BRCA: Breast invasive carcinoma, CESC: Cervical squamous cell carcinoma and endocervical adenocarcinoma, CHOL: Cholangiocarcinoma, COAD: Colon adenocarcinoma, DLBC: Lymphoid Neoplasm Diffuse Large B-cell Lymphoma, ESCA: Esophageal carcinoma, GBM: Glioblastoma multiforme, HNSC: Head and Neck squamous cell carcinoma, KICH: Kidney Chromophobe, KIRC: Kidney renal clear cell carcinoma, KIRP: Kidney renal papillary cell

carcinoma, LAML: Acute Myeloid Leukemia, LGG: Brain Lower Grade Glioma, LIHC: Liver hepatocellular carcinoma, LUAD: Lung adenocarcinoma, LUSC: Lung squamous cell carcinoma, MESO: Mesothelioma, OV: Ovarian serous cystadenocarcinoma, PAAD: Pancreatic adenocarcinoma, PCPG: Pheochromocytoma and Paraganglioma, PRAD: Prostate adenocarcinoma, READ: Rectum adenocarcinoma, SARC: Sarcoma, SKCM: Skin Cutaneous Melanoma, STAD: Stomach adenocarcinoma, TGCT: Testicular Germ Cell Tumors, THCA: Thyroid carcinoma, THYM: Thymoma, UCEC: Uterine Corpus Endometrial Carcinoma, UCS: Uterine Carcinosarcoma, UVM: Uveal Melanoma

Figure S2

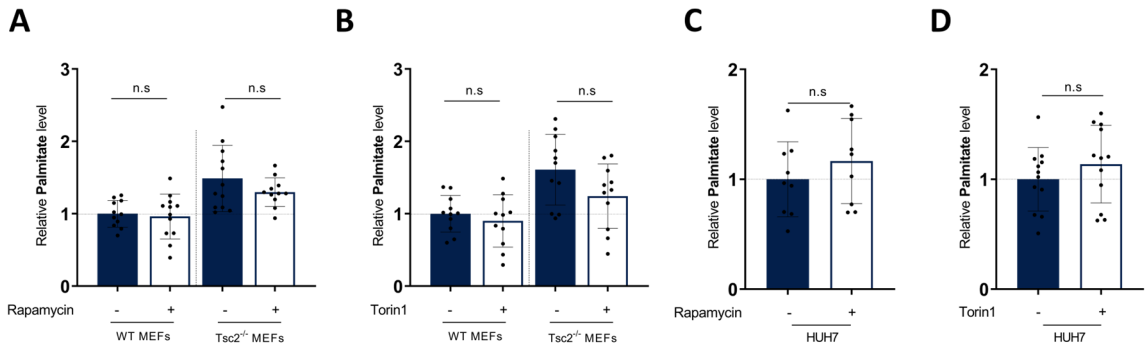

Figure S2: mTOR inhibition does not alter palmitate levels, Related to Figure 2 and Figure 3

(A, B) Relative palmitate level upon treatment with DMSO (A, N=12, B, N=11), rapamycin (A) (20 nM, 72 h, N=12) or Torin1 (B) (40 nM, 72 h, N=11) in WT and Tsc2$^{-/-}$ MEFs. Bar graphs are presented as mean ± SD from biological independent samples. Statistical testing was performed by a two-sided unpaired Student's t test.

(C, D) Relative palmitate level upon treatment with DMSO (C, N=9, D, N=12), rapamycin (C) (20 nM, 72 h, N=9) or Torin1 (D) (40 nM, 72 h, N=12) in HUH7 cancer cells. Bar graphs are presented as mean ± SD from biological independent samples. Statistical testing was performed by a two-sided unpaired Student's t test.

Figure S3

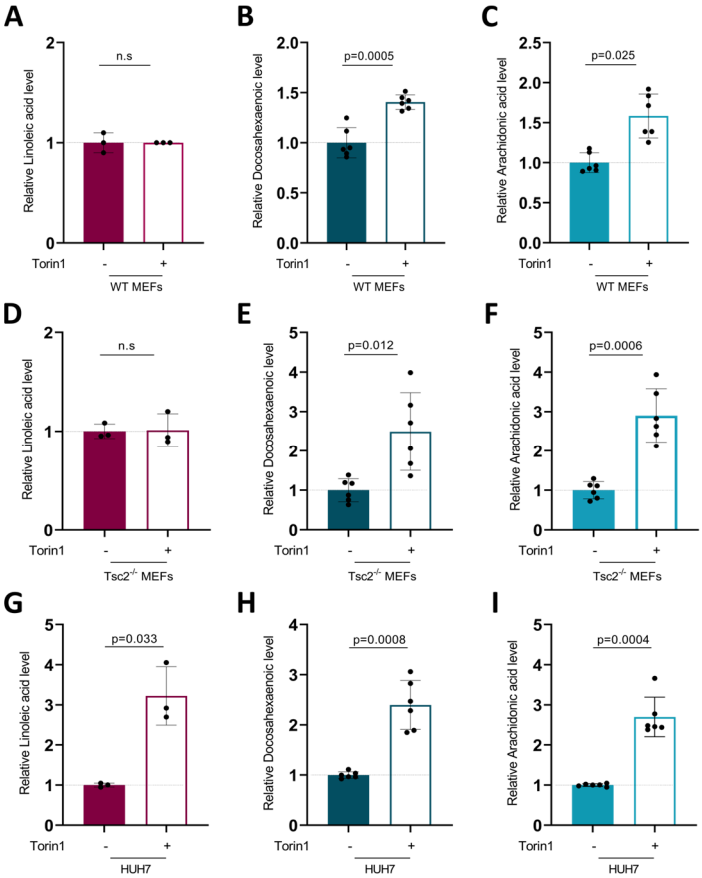

Figure S3: mTOR inhibition results in elevated polyunsaturated fatty acid levels, Related to **Figure 2** and **Figure 3**

(A-C) Relative levels of linoleic acid (**A**), docosahexaenoic acid (**B**) and arachidonic acid (**C**) in the wildtype (WT) MEFs upon treatment with DMSO or Torin1 (40 nM, 72 h, **A**, N=3, **B-C**, N=6). Bar graphs are presented as mean ± SD from biological independent samples. Statistical testing was performed by a two-sided unpaired Student's t test.

(D-F) Relative levels of linoleic acid (**D**), docosahexaenoic acid (**E**) and arachidonic acid (**F**) in the $Tsc2^{-/-}$ MEFs upon treatment with DMSO or Torin1 (40 nM, 72 h, **D**, N=3, **E-F**, N=6). Bar graphs are presented as mean ± SD from biological independent samples. Statistical testing was performed by a two-sided unpaired Student's t test.

(G-I) Relative levels of linoleic acid (**G**), docosahexaenoic acid (**H**) and arachidonic acid (**I**) in the HUH7 cancer cells upon treatment with DMSO or Torin1 (40 nM, 72 h, **G**, N=3, **H-I**, N=6). Bar graphs are presented as mean ± SD from biological independent samples. Statistical testing was performed by a two-sided unpaired Student's t test.

Figure S4

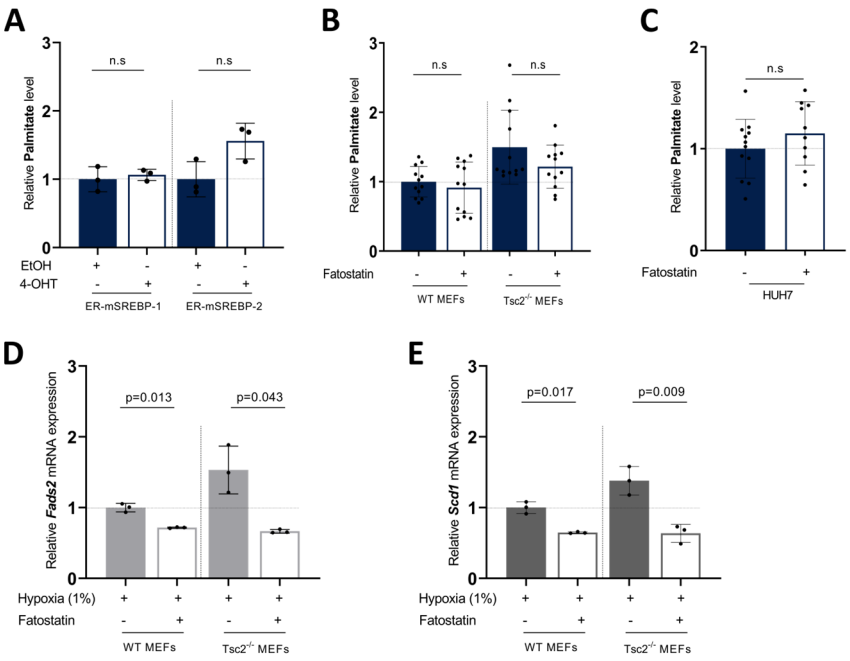

Figure S4: SREBP modulation does not alter palmitate level and regulates *Fads2* and *Scd1* transcription in hypoxia, Related to **Figure 4**

(A) Relative palmitate level was determined in U87 cells stably expressing ER-mSREBP-1 or ER-mSREBP-2. Cells were treated with 100 nM 4-OHT or solvent for 24 h in medium containing 10% FBS (N=3). Bar graphs are presented as mean ± SD from biological independent samples. Statistical testing was performed by a two-sided unpaired Student's t test.

(B, C) Palmitate level upon treatment with DMSO (N=12) or fatostatin (10 µM, 72 h, **B**, N=12, **C**, N=10) in WT and Tsc2$^{-/-}$ MEFs (**B**) and in HUH7 cancer cells (**C**). Bar graphs are presented as mean ± SD from biological independent samples. Statistical testing was performed by a two-sided unpaired Student's t test.

(D, E) *FadsS2* (**D**) and *Scd1* (**E**) mRNA expression in WT and Tsc2$^{-/-}$ MEFs cells treated with fatostatin (10 µM, 48 h, N=3) combined with hypoxia (1% O_2). Relative mRNA levels were determined by qPCR. Bar graphs are presented as mean ± SD from biological independent samples. Statistical testing was performed by a two-sided unpaired Student's t test.

Table S5: qPCR primer sequences list, Related to KEY RESOURCES TABLE

	Gene	Forward (5'-3')	Reverse (5'-3')
Human	*FADS2*	GACCACGGCAAGAACTCAAAG	GAGGGTAGGAATCCAGCCATT
	SCD1	TCTCTGCTACACTTGGGAGC	GAGCTTTGTAAGAGCGGTGG
	FADS2 (Site A)	TCTGCTGATCGCTGTGGAAACT	TCAGCCCTCCCGCTATGGACTTT
	FADS2 (Site B)	TGGAGGCAAAAGTCCATAGC	GATCCCTGGCTTCCCAGT
	ACTB	GCCTCGCCTTTGCCGAT	CGCGGCGATATCATCATCC
	RPL19	ACCCCA ATGAGACCA ATG AA	CGCAAAATCCTCATTCTCCT
Mouse	*Fads2*	ATAGTAGCTGATGGCCCAAGC	AGCCCCTTGAGTATGGCAAG
	Scd1	CGCTCTTTACCCTTTGCTGG	AAGAACTGGAGATCTCTTGGAGC
	Rpl19	CAGGCATATGGGCATAGGGAA	TGCCTTCAGCTTGTGGATGT